

Electronic materials with nanoscale curved geometries

Paola Gentile,^{1,2} Mario Cuoco,^{1,2} Oleksii M. Volkov,³ Zu-Jian Ying,⁴
Ivan J. Vera-Marun,^{5,6} Denys Makarov,³ and Carmine Ortix^{2,7}

¹*CNR-SPIN c/o Università di Salerno, I-84084 Fisciano (Salerno), Italy*

²*Dipartimento di Fisica, Università di Salerno, I-84084 Fisciano (Salerno), Italy*

³*Helmholtz-Zentrum Dresden-Rossendorf, Institute of Ion Beam Physics and
Materials Research, Bautzner Landstrasse 400, 01328 Dresden, Germany*

⁴*School of Physical Science and Technology, Lanzhou University, Lanzhou 730000, China*

⁵*Department of Physics and Astronomy, University of Manchester, Manchester M13 9PL, United Kingdom*

⁶*National Graphene Institute, University of Manchester, Manchester M13 9PL, United Kingdom*

⁷*Institute for Theoretical Physics, Center for Extreme Matter and Emergent Phenomena,
Utrecht University, Princetonplein 5, 3584 CC Utrecht, Netherlands*

Research into electronic nanomaterials has recently seen a growing focus into the synthesis of structures with unconventional curved geometries including bent wires in planar systems and three-dimensional architectures obtained by rolling up nanomembranes. The inclusion of these geometries has led to the prediction and observation of a series of novel effects that either result from shape-driven modifications of the electronic motion or from an intrinsic change of electronic and magnetic properties due to peculiar confinement effects. Moreover, local strains often generated by curvature also trigger the appearance of new phenomena due to the essential role played by electromechanical coupling in solids. Here we review the recent developments in the discovery of these shape-, confinement- and strain-induced curvature effects at the nanoscale, and discuss their potential use in electronic and spintronic devices.

I. INTRODUCTION

The electronic, magnetic and optical properties of materials acquire distinctive features when confined to two-dimensional sheets, one-dimensional nanowires and zero-dimensional quantum dots. As one progresses from an extended bulk solid to these nanostructures, size and quantum confinement effects become pervasive and strongly alter the material responses. In recent years, progresses in various nanostructuring techniques have enabled to expand electronic nanomaterials into the third dimension via the synthesis of nanoarchitectures that are made of constructs of two and one-dimensional nanomaterials. These advances have been largely triggered by the quest for high-density electronic memory and logic devices with a substantial increase in performance and reliability¹⁻³. Three-dimensional nanoarchitectures also address technological challenges in, for instance, three-dimensional magnetic sensing⁴ and CMOS compatible magneto-impedance sensorics⁵.

However, the realization of this new family of devices, which often require elements with curved geometric shapes such as spiralling tubes or helices, also pose theoretical and experimental questions. First, can the curved geometry lead to novel variations of the fundamental properties of the material structure? Second, can these unprecedented physical properties be used to design electronic devices with different and even superior functionalities than the existing ones?

At the fundamental level, a curved geometric shape introduces a new length scale crucial for the properties of the material structure: the characteristic radius of curvature. Consider for instance a diffusive electronic transport channel that is geometrically deformed. When the radius of curvature becomes comparable to the electronic mean free path, the charge and spin transport characteristics determined by the many (spin-flip) scattering events can be influenced by the bent electron

trajectories imposed by the curved shape of the channel. Beside these classical shape effects on the electronic motion, curvature can also drive, via confinement and electromechanical coupling to inhomogeneous strain fields, strong deviations of the material intrinsic electronic properties. This occurs whenever the curvature radius approaches the de Broglie wavelength of the electrons near the Fermi level. In a similar manner, the ground state and the elementary excitations of materials exhibiting long-range order, like magnets and superconductors, can be geometrically tuned when the magnetic length or the superconducting coherence length are comparable to the curvature radius.

Nanoscale geometry-induced effects can therefore pervade the physical properties of essentially all materials and endow them with characteristics that would be hardly possible to achieve in conventional “flat” structures of the same material. The focus of this Review is to highlight the physical origin of these new shape, confinement, and strain-induced functionalities, and how to exploit them in electronics, as well as in spin and even superconducting electronics.

II. CLASSICAL SHAPE EFFECTS

A. Curved spintronics

A first example of geometry-induced effects results from the structural inhomogeneities that can be engineered in curved electronic channels. Fabrication of curved channels using a (non-planar) shaped substrate that acts as a template yields thicknesses with a local profile in one-to-one correspondence with the geometry. Specifically, and as evidenced in Fig. 1(a), the thickness of a curved channel is strongly reduced in the regions of large curvature gradient. This characteristic can be used to efficiently tune the electrical properties of the system

Curved Spintronics

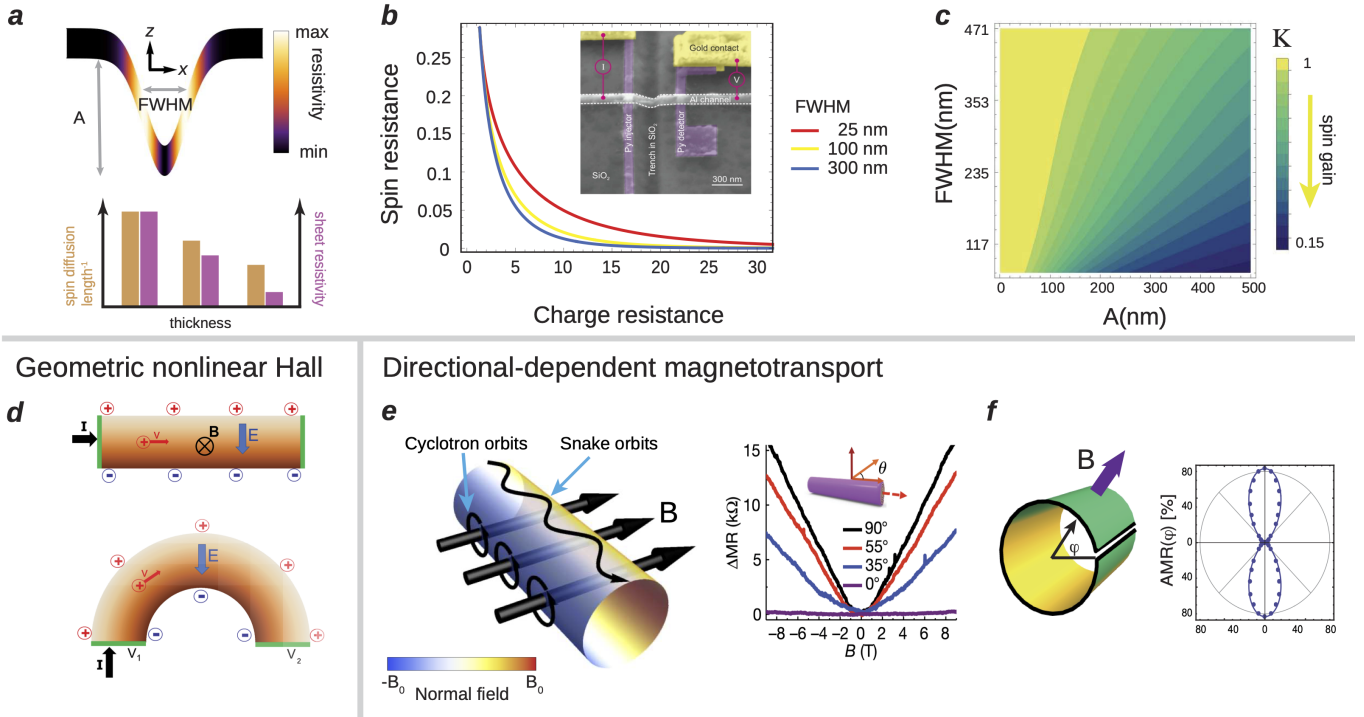


Figure 1. Classical shape effects (a) Sketch of an electronic channel grown on a trenched substrate with given height (A) and full width at half-maximum (FWHM). The thickness inhomogeneity along the channel creates a local resistivity distribution. There is a different scaling between the sheet resistivity $\rho(t)/t$ and the inverse of the spin diffusion length $\rho(t)$. (b) Room temperature spin resistance measured in a non-local spin valve vs. the charge resistance of a curved Al channel grown on trenched substrates of different FWHM. The SEM image of the spin-valve is adapted from Ref.⁶. (c) Color map of the curvature factor K regulating the exponential decrease rate of the spin signal in a non-local spin valve with a trenched channel [see Ref.⁶], and injector-detector distance $L = 500$ nm. Values of the curvature factor $K < 1$ imply a gain in the spin signal relative to the charge resistance. (d) Sketch of the surface charges induced in the classical Hall effect, and the surface charges in a curved wire that produce the electric field accelerating the carriers centripetally. (e) Color map of the normal component of a transversal magnetic field in a nanotube and the corresponding electronic semiclassical trajectories. The right panel shows the magnetoresistance measured in $\text{SnS}_2/\text{WSe}_2$ superlattices by tilting an axial magnetic field in the transversal direction [adapted from Ref.⁷]. (f) In carbon nanoscrolls with open geometries, a purely transversal magnetic field yields a strongly directional-dependent magnetoresistance [adapted from Ref.⁸].

when the nanoscale thickness is comparable to the electronic mean free path. Even if quantum effects do not come into play due to the smallness of the de Broglie wavelength, classical size effects consisting in an increase of the resistivity due to diffusive scattering at the channel and grain boundaries⁹, transform the shape-driven thickness inhomogeneities into an enhanced local nanoscale resistivity [see Fig. 1(a)].

In addition, the local sheet resistance $\rho(t)/t$ decreases faster than the resistivity $\rho(t) \propto 1/t$ as the thickness t increases [see Fig. 1(a)]. This different scaling can be exploited in curved metallic nanochannels with engineered local thickness of a few tens of nanometers when used as pure spin transport channels^{10–12}. Metallic materials form the basis of current spintronic technologies. In addition, the dominant spin relaxation mechanism corresponds to the so-called Elliot-Yafet mechanism^{13,14}. This dictates that the spin diffusion length is strictly locked to the resistivity of the metallic channel. The distinct scaling between local sheet resistance and resistivity consequently allows to control independently

the charge and spin transport properties of a curved metallic channel. Such independent tuning has been realized⁶ in lateral non-local spin valves [c.f. Fig. 1(b)]. A given spin valve signal – defined by the difference in the nonlocal resistance between parallel and antiparallel magnetic states of the injector and detector electrodes – can be obtained for different values of the channel charge resistance [c.f. Fig. 1(b)] and *vice versa*, in stark contrast with the case of conventional “flat” channels where instead the spin and charge resistances are locked to each other. In addition, for devices with the same lateral footprint and at given charge resistance, the spin signal of a flat channel is always smaller than the electric response obtained using a curved channel. This is encoded in a curvature factor [c.f. Fig. 1(c)] that quantifies the gain in the spin signal obtained using the intrinsic inhomogeneity of the curved channel. This generalized advantage combined with the independent tuning of charge and spin responses are of immediate relevance when considering practical implementation of spintronics: the use of geometric curvature to control

on demand spin and charge impedances in multiterminal devices adds a novel approach for their efficient integration with complementary metal oxide semiconductor transistors.

B. Geometric nonlinear Hall effect

Geometric curvature can also lead to classical shape effects that directly derive from the charge motion in the tangential curved direction of the channel and can therefore appear even in planar structures. These are therefore completely different from the boundary scattering effect in the thickness direction at the basis of curved spintronics. In curved channels, charge carriers are forced to follow paths that in conventional flat channels typically require the presence of external electromagnetic fields. Consider for simplicity a planar curved wire taking the shape of a semicircular annulus¹⁵. Injection of a current in this channel necessarily leads to the appearance of a transverse electric potential: the current has to be accelerated radially to follow the circular path. This creates surface charges similar in nature to those of the classical Hall effect [c.f. Fig. 1(d)] even if a perpendicular magnetic field is absent. The ensuing transverse potential is quadratic in the current density, as required by time-reversal invariance, and can be thus regarded as a purely geometric nonlinear ‘‘Hall’’ effect. The quadratic dependence on the injected current implies that an ac current with frequency ω will yield a transverse potential with 2ω frequency. It is thus different than the transversal response occurring as a result of fluctuations in resistivity due to Joule heating since the latter gives rise to potential at higher harmonics. Using lock-in amplifiers, it is also possible to filter out other Hall-like contributions due, for instance, to spurious magnetic fields that yield potentials with ω frequency. Adopting this strategy, signatures of the geometric non-linear Hall effect have been individuated in graphene circular wires¹⁵.

C. Directional-dependent magnetotransport

The appearance of tortuous electronic trajectories in curved channels becomes even richer in the actual presence of external magnetic fields. This can be shown by considering the perhaps most common example of a nanostructure with curved geometry – carbon nanotubes¹⁶ – in the presence of a transversal magnetic field. Charge carriers in carbon nanotubes respond primarily to the normal component of the externally applied magnetic field, which, as shown in Fig. 1(e), changes sign at opposite side of the tube and averages out. When the cyclotron radius associated to the externally applied magnetic field $R_{cycl} = m^*v_F/(eB)$, with v_F being the Fermi velocity and m^* a density-dependent dynamical mass¹⁷, is larger than the nanotube radius, the electronic trajectories correspond to helix-like orbits completely wrapping the tube. A direct computation of the magnetoconductance in the diffusive regime⁸ has revealed that these classical helical orbits yield, even in a single channel model, a quadratic longitudinal magnetoresistance experimentally observed in nanotube bundles¹⁸ and multi-walled carbon nanotubes¹⁹. In the regime where the cy-

clotron radius is smaller than the carbon nanotube radius, the nature of the classical electron trajectories changes qualitatively. The externally applied magnetic field is indeed large enough to allow for the formation of cyclotron orbits completely localized in the regions where the surface normal is parallel to the magnetic field²⁰ [c.f. Fig. 1(e)]. These cyclotron orbits do not contribute to the magnetoconductance contrary to the snake orbits that are instead naturally formed in nanotube regions where the normal component of the magnetic field changes its sign²¹. The snake orbits contribution to the magnetoresistance is characterized by a \sqrt{B} power-law dependence⁸ explicitly shown in transport measurements¹⁹. A similar unconventional linear magnetoresistance has been also recently observed in a different material system: van der Waals SnS₂/WSe₂ heterostructures rolled-up into tubes⁷. In this radial superlattice the magnetoresistance strongly decreases by tilting the magnetic field towards the axial direction [see the right panel of Fig. 1(e)] thus suggesting the formation of snake orbits as responsible for this phenomenon.

The imprint of snake orbits on the magnetotransport properties of tubular nanostructures becomes even more apparent when considering the open geometry of carbon nanoscrolls^{22,23} – spirally wrapped graphite layers that unlike carbon nanotubes have overlapping fringes. In carbon nanoscrolls the density of snake orbits depends crucially on the direction of the transversal magnetic field. When the external magnetic field is directed towards the open edges there is a proliferation of snake orbits for the simple reason that the charge carriers feel an additional sign change of the effective normal magnetic field, as compared to the case in which the external magnetic field is directed orthogonal to the open edges. For instance in a single winding rolled-up open tube, the normal component of the magnetic field changes sign once or twice depending on the transversal magnetic field direction [c.f. Fig. 1(f)]. Consequently, carbon nanoscrolls can display a strongly directional dependent magnetoresistance similar in its functional dependence to the anisotropic magnetoresistance of spin-orbit coupled magnetic materials. The magnitude of this effect, which is the immediate result of the broken rotation symmetry of the tubular structure, has been predicted⁸ to be remarkably large in single winding carbon nanoscrolls as it can reach 80% [c.f. Fig. 1(f)].

III. CONFINEMENT-INDUCED CURVATURE EFFECTS

A. Ballistic transport

Characteristic fingerprints of the formation of snake orbits can be also encountered in the ballistic transport regime of traditional semiconducting materials with mean free paths much larger than the curvature radii. An important example is represented by core-shell nanowires²⁵: systems consisting of a conducting, *e.g.* InAs, shell surrounding a, *e.g.* GaAs, core²⁶. In their electronic band structure, the inhomogeneous radial component of the magnetic field leads to Landau states condensed at small wavenumbers. These states are connected for larger momenta to dispersive states corresponding in a semi-

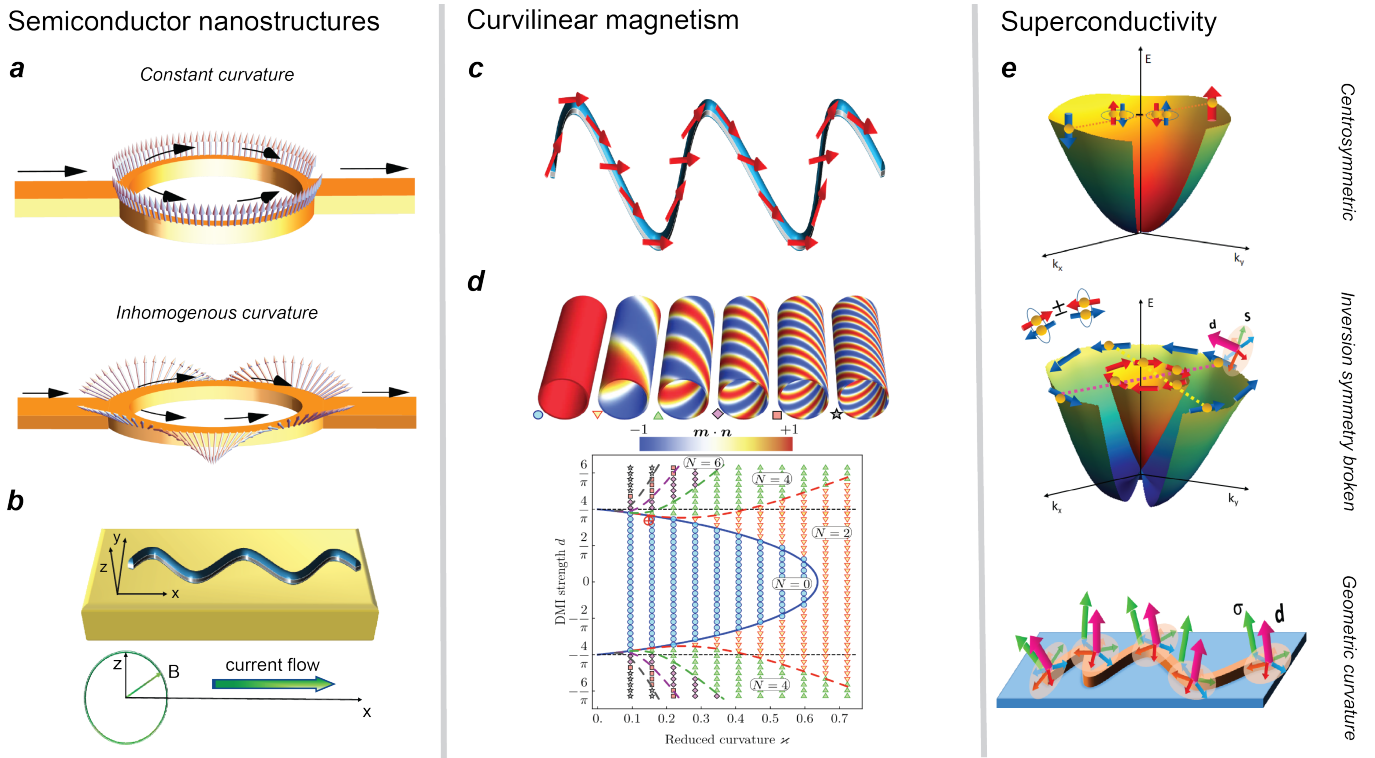


Figure 2. **Confinement-induced effects** (a) Schematics of the spin textures realized in circular (top) and shape-deformed (bottom) Rashba spin-orbit interferometers. In the latter, there is a spin-torque that leads to tangential spin components. (b) Top: Schematic view of a semiconducting one-dimensional channel patterned in a serpentine shape at the mesoscopic scale. Bottom: Diagram of the pumping induced by the rotation of an external magnetic field. (c) Sketch of the magnetization textures (red arrows) along a bent magnetic wire with tangential anisotropy. (d) Equilibrium magnetic states in magnetic nanotubes with Dzyaloshinskii-Moriya interaction (DMI). Varying the strength of the DMI interaction and the curvature radius of the tube results in a phase diagram where the stable magnetic state is represented by the symbol associated to the nanotube [adapted from Ref. ²⁴]. (e) Superconductors with center of inversion usually have an order parameter that is a spin-singlet state (top panel). In acentric materials, spin-singlet Cooper pairs are expected to be converted into a mixture of spin-singlet and spin-triplet states. These are characterized by a d -vector that is generally parallel to the helical single electron spin σ . The spin s of the Cooper pairs lies in the plane orthogonal to the d vector. In one-dimensional dimensional systems a texture of the d vector is generated in real space by curvature effects.

classical analysis to the snake orbits. Such snake states are situated at the bottom of the energy spectrum. Consequently, they represent the main actors in the quantum transport at low chemical potential²⁷. Numerical calculations have shown that snake states result in peaks in the quantum conductance of core-shell nanowires, with the peak amplitude that can be tailored by adjusting the position of the metallic contacts with respect to the alignment of the transversal magnetic field. Similar conductance oscillations due to snake states have been also reported in graphene p-n junctions in the ballistic regime^{28,29}.

Semiconducting core-shell nanowires are however often grown with hexagonal cross sections and edges between different crystallographic facets that are rounded to form regions with finite curvature. In these regions, the corresponding local curvature radius can be small enough to be comparable to the de Broglie wavelength of the carriers, thus allowing to probe the quantum geometric potential arising from confinement on curved surfaces [see Box 1]. This quantum geometric potential consists of a series of square wells³⁰ and thus makes the rounded edges of a prismatic core-shell nanowire regions of preferred localization. Such intrinsic curvature-induced lo-

calization has a strong interplay with the formation of snake orbits in the presence of a transversal magnetic field. Consider first a transversal magnetic field orthogonal to one of the facets of the core-shell nanowire: it will favour the formation of snake states on the two perpendicular edges enhancing their charge localization as compared to the other edges. On the other hand, for a magnetic field pointing toward one edge, snake states will form along the facets and counteract the tendency to localize the electronic charge at the nanowire edges. This different charge localization mechanism is then reflected in a ballistic directional-dependent magnetoresistance.

An ideal three-dimensional topological insulator (TI) nanowire can be thought as of another material structure consisting of a conducting curved shell surrounding an insulating bulk. In the diffusive regime, the presence of an axial magnetic field gives rise to periodic Altshuler, Aronov and Spivak (AAS) magnetoconductance oscillations originating from weak antilocalization. These AAS oscillations, with period $h/(2e)$, are substituted in the (quasi)ballistic transport regime by h/e periodic Aharonov-Bohm (AB) oscillations that are instead the result of the existence of the so-called

perfectly transmitted mode. In curved geometries the single (spin-momentum locked) Dirac cone theory for the surface of a TI acquires a spin connection term that yields a Berry phase and consequently a gapped spectrum. However, a magnetic flux of half a flux quantum identically cancels the Berry phase and restores a gapless spectrum with an odd number of modes. Therefore, a perfectly transmitted mode with conductance e^2/h occurs³¹. AB magnetoconductance oscillations have been experimentally observed in Bi_2Se_3 ³² and HgTe nanowires³³. Superimposing a local variation of the nanowire curvature radius, *i.e.* considering nanocones, has been recently predicted³⁴ to lead to other intriguing mesoscopic transport phenomena such as resonant transmission through Dirac Landau levels.

B. Spin-orbit coupled semiconducting materials

Semiconducting nanomaterials also exhibit curvature effects that are due to relativistic corrections. The interplay between spin-orbit coupling and curvature leads to the appearance of complex spin-textures without counterparts in conventional “flat” nanostructures. This is because in the rest frame of the electrons, the effective spin-orbit field has a geometric component^{35,36} [see Box 1] governed by the local geometric curvature. This geometric spin-orbit field has been directly probed in a simple class of nanostructures with curved geometries: semiconducting quantum rings with Rashba spin-orbit coupling^{37,38}. In these systems, the out-of-plane tilt of the spin textures [see Fig. 2(a)] gives characteristic fingerprints in the conductance interference patterns^{39,40}.

The conductance modulations are regulated by the Aharonov-Anandan geometric phase – the non-adiabatic analog of the Berry phase – which is in one-to-one correspondence with the spin textures³⁶. Importantly, the quasi-periodic modulations can be additionally tuned by means of external planar magnetic fields. The geometric spin-orbit field has remarkable consequences in geometries with inhomogeneous curvature³⁶. In this case, the spin-orbit field exerts a torque on the electronic spin which then acquires a finite component parallel to the electron propagation direction [see Fig. 2(a)]. The ensuing complex three-dimensional spin textures prove local curvature control of the Aharonov-Andan geometric phase and can be directly probed in interferometric spintronic devices with unconventional geometries such as ellipses and squares⁴¹.

The geometric spin torque has an important role also in zigzag-shaped nanowires where the local geometric curvature has a periodic profile⁴². The miniband structure of this geometric superlattice is indeed characterized by the presence of minigaps opened by spin-orbit coupling at unpinned points in the mini Brillouin zone. The periodic buckling of a nanowire therefore induces a metal-insulator transition defining a geometric transistor switch. Additionally, the insulating states generally display Tamm-Shockley in-gap end modes⁴³. The concomitant presence of the confinement-induced quantum geometric potential and the geometric spin torque can be also exploited to design new solid state electronic se-

tups. For instance, it has been theoretically proposed that a zigzag-shaped nanowire with strong Rashba spin-orbit coupling can operate as a topological charge pump [see Fig. 2(b)] in the complete absence of superimposed oscillating local voltages⁴⁴, differently from the conventional pumping protocol in one-dimensional systems originally introduced by Thouless⁴⁵. To operate the device, one uses an external rotating planar magnetic field – generated for instance by running current pulses in two perpendicular conductors with a $\pi/2$ phase shift – that serves as the periodic ac perturbation driving the charge pumping. The time-dependent Zeeman coupling acting on the spin textures realized by the geometric spin-orbit torque results ultimately in a sliding superlattice charge potential. Combining the latter with the charge gap opening mechanism provided by the quantum geometric potential leads to states with a non-trivial Berry curvature in the synthetic two-dimensional mini-Brillouin zone, which, when integrated, yields a “dynamical” non-zero Chern number⁴⁶. Hence, in each pumping period the device pumps two electronic charges with the quantization that is topologically protected against external perturbations, and can be relevant for metrological purposes.

C. Curvilinear magnetism

Curvature effects can be also exploited for novel spintronic device concepts relying on magnetic domain wall motion. In magnetic wires with helical shapes, geometry offers unconventional means to control Rashba spin torque-driven⁴⁷ as well as spin current-driven⁴⁸ domain wall dynamics. This is because the magnetic equilibrium state in thin films and wires is directly influenced by geometric curvature^{49,50}. For instance, in a buckled magnetic wire with tangential anisotropy the magnetization vector generally displays local deviations from the tangential direction [see Fig. 2(c)]. These effects are due primarily to the magnetic exchange energy, which yields an effective Dzyaloshinskii-Moriya interaction (DMI) and an effective magnetic anisotropy [see Box 1] as a result of the confinement on curved geometries. The existence of this effective antisymmetric exchange interaction has important consequences also on the existence and stability of modulated magnetic phases whenever the geometric curvature is comparable to the exchange magnetic length. Consider for instance a flat ultrathin film with an intrinsic DMI interaction. It is known that there exists a critical DMI strength separating homogeneous and periodic magnetization distributions⁵¹. If now the ultrathin film is bent with a constant curvature radius so as to create a magnetic nanotube, the effective curvature-induced DMI will renormalize the critical strength at which the modulated phase sets in²⁴. In particular, by decreasing the curvature radius modulated phases can be stabilized by the geometry and appear even for vanishing intrinsic DMI strength [see Fig. 2(d)]. Similar features are encountered when considering skyrmions in magnetic nanotubes, which have been predicted to stably exist already in moderate magnetic field ranges⁵².

Curvature effects yield peculiar features also in the dynam-

ics of domain walls (DWs) in magnetic nanotubes. The configuration of a DW in a magnetic nanotube is characterized by the presence of a core-less vortex structure in the region separating the two oppositely magnetized domains. The two possible vorticities then distinguish two different DW configurations which are energetically degenerate but have different dynamical properties. Because of the presence of a finite radial magnetization component, an applied magnetic field exerts a torque on the DW. This, in turn, affects the radial magnetization itself. Whether the DW is distorted with a compression or enhancement of the radial magnetization depends on the handedness of the system defined by combining the vorticity of the DW with the magnetic field vector direction⁵³. This chiral dependent distortion ultimately modulates the motion of the DWs. Micromagnetic calculations based on the Landau-Lifshitz-Gilbert equation show that the velocity of the DWs is strongly dependent on the chirality. Importantly, also the stability of the DW displays chiral-dependent features. Certain chiral DWs have a completely suppressed Walker breakdown⁵⁴: the collapse of the DW structure at a critical velocity, and one of the main complications for the optimization of memory device and logic gates based on fast and controlled DW motion. This is primarily due to the fact that breakdown of a DW in a tube involves a vortex-antivortex pair creation contrary to the single vortex-mediated breakdown of DW in flat thin films. Based on this topological constraint, DWs generally have a strongly enhanced stability when guided in tubular nanostructures.

Chiral symmetry breaking effects have been predicted⁵⁵ and more recently observed⁵⁶ in magnonics. Spin waves – magnetic excitations that hold potential in information processing – acquire a peculiar asymmetric dispersion in magnetic nanotubes with an equilibrium state in which the magnetization rotates around the circumference of the tube. Specifically, spin waves of same frequency propagating in different directions are characterized by different wavelengths. Since the rotating magnetization together with the propagation direction defines a handedness, the occurrence of this phenomenon implies a chiral symmetry breaking. Importantly, this effect, occurring in conventional thin film geometries only in the presence of intrinsic DMI interaction, does not originate from the exchange interaction but rather from the non-local dipole-dipole interaction.

D. Superconducting electronics

Recent theoretical studies have suggested that the effective spin torques activated by geometry might affect also electronic pairing and possibly lead to new functionalities in superconducting spintronics. One of the paradigms of superconducting spintronics is to exploit spin-triplet Cooper pairs since they can carry angular momentum without energy dissipation, and thus can be functionalized to yield spin-polarized supercurrents for ultrahigh energy-efficient storage and transfer of information⁵⁷. Spin-triplet pairing has a vectorial nature and can be typically encoded in the so-called \mathbf{d} -vector⁵⁸ whose components correspond to the zero spin projections

of the triplet state along the symmetry axes [see Box 1]. A crucial challenge in the area of superconducting spintronics is to achieve control mechanisms and devise systems that are able to convert spin-singlet into spin-triplet electron pairs since spin-singlet superconductors are more abundant in nature. This issue has been largely investigated by engineering superconductor-magnet heterostructures with suitably designed non-collinear magnetic patterns^{59–61} and more recently by considering spin-orbit coupling without breaking time-reversal symmetry⁶². In this context, systems with Rashba spin-orbit coupling due to structural inversion asymmetry are particularly appealing.

In two dimensions the lack of inversion symmetry removes the spin degeneracy of the Bloch states and a spin texture develops in the Brillouin zone due to the Rashba interaction that couples the electron spin with the crystal wave vector⁶³. For Cooper pairs, this symmetry reduction forces the occurrence of a mixing of spin-singlet and spin-triplet pairing at the Fermi level. Moreover, due to the spin anisotropy, the spin-triplet \mathbf{d} vector follows the electron spin orientation⁶⁴ resulting into a helical pattern [see Fig. 2(e)]. If at a given momentum k at the Fermi level the electron spin points along the y direction, \uparrow_y , with the time reversal partner \downarrow_y at $-k$, the resulting spin-triplet configuration can only be with vanishing total spin projection along the y orientation thus corresponding to the d_y component. In analogy to the spin-triplet texture occurring in momentum space along the Fermi line, a variation of the \mathbf{d} -vector orientation occurs in real space when geometric curvature is present⁶⁵. As discussed above, the geometric spin-orbit torque yields local variations of the electron spin orientation³⁶. Hence, to avoid pair breaking, the spin-triplet configuration has to follow the spin anisotropy by twisting the \mathbf{d} vector according to the curvature of the electronic channel [see Fig. 2(e)]. Crucially, the reconstruction depends on the ratio between the geometric curvature and the superconducting coherence length. Then, the combined presence of geometric curvature and spin-orbit coupling has the effect to generate spin-triplet pairs with an orientation that is substantially dictated by the profile of the confining potential. These mechanisms can lead to striking effects in superconducting electronics. As a direct example, the Josephson effect can be mechanically controlled both in the amplitude and phase of the supercurrent by geometrically curving the superconducting electrodes⁶⁶.

IV. STRAIN-DRIVEN CURVATURE EFFECTS

A. Strain-induced geometric potential

In nanosystems with curved geometries electromechanical coupling leads to effects that often coexist and amplify the confinement-induced curvature effects discussed above. A key property of bent nanostructures fabricated using strain engineering methods is the presence of local strain fields varying on the nanoscale⁷¹. In insulators, the presence of these strain gradients is at the basis of the flexoelectric effect – an electromechanical coupling that, contrary to piezoelectricity,

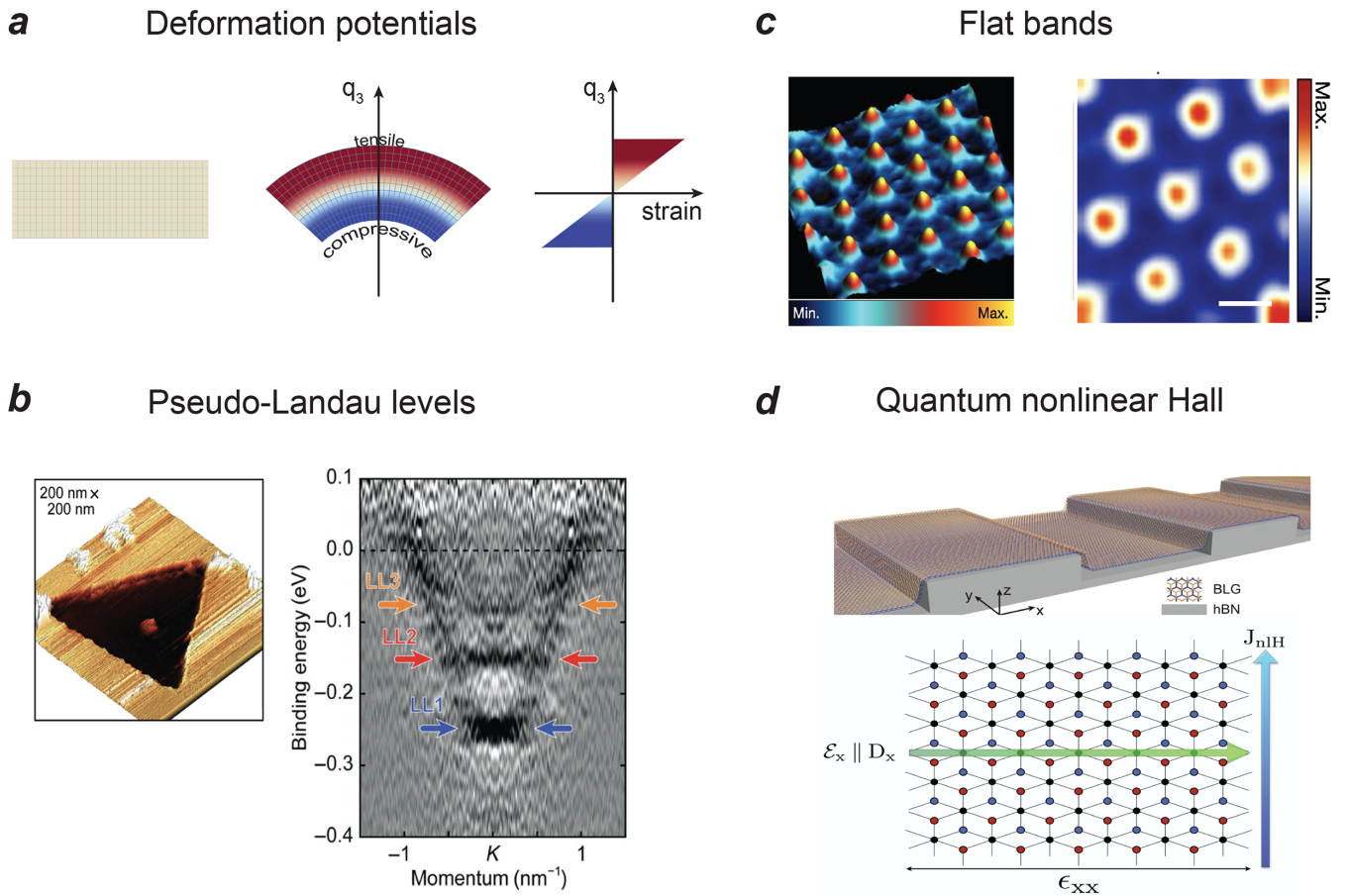


Figure 3. Strain-induced effects (a) Bending a flat nanostructure creates a strain gradient with regions under compressive and tensile strain separated by the mechanical neutral plane $q_3 \equiv 0$. (b) Graphene grown on SiC substrates displays nanoprims as evidenced in atomic force microscopy tomography where one Si layer is missing. The formation of pseudo-Landau levels in the strained nanoprims can be observed even at room temperature using angle-resolved photoemission spectroscopy. Adapted from Ref.⁶⁷. (c) Left: STM topography. Right: Measured dI/dV maps at energy corresponding to one of the flat-band regions created by the buckling-induced periodic pseudo-magnetic field. Adapted from Ref.⁶⁸. (d) Top: Artificially corrugated bilayer graphene (BLG) on a patterned hexagonal boron nitride substrate. Adapted from Ref.⁶⁹. Bottom panel: Top view of the regions where bilayer graphene is strained. A nonlinear Hall current J_{nIH} is generated under the application of an electric field E_x parallel to the dipole D_x . Adapted from Ref.⁷⁰.

is universal and symmetry-allowed in all solids⁷². Strain gradients spontaneously generated in curved nanostructures yield remarkable effects also in semiconducting materials. According to the linear potential deformation theory⁷³, a local strain yields a shift of the conduction (valence) band edges, and therefore corresponds to a local potential attracting the charge carriers towards the maximally strained regions [see Fig. 3(a)]. This potential is therefore directly proportional to the local geometric curvature with a corresponding characteristic energy scale that lies in the eV range for conventional semiconductors. Using an adiabatic separation of fast and slow quantum degrees of freedom⁷⁴, it can be shown that this local potential ultimately yields a strain-induced geometric potential of the same functional form of the confinement-induced quantum geometric potential but strongly, often gigantically, boosting it. Such large enhancement of curvature effects renders the phenomena predicted in curved nanostructures, ranging from winding-generated bound states in rolled-

up nanotubes⁷⁵ to topological band structures in systems constrained to periodic minimal surfaces⁷⁶, observable above the sub-Kelvin energy scale. In micrometer sized wrinkled ribbons of GaAs, for instance, curvature-induced localized end states have been predicted to be observable up to a few Kelvin if local strain fields are explicitly taken into account⁷⁷.

B. Gauge fields in Dirac materials

Strain fields yield remarkable effects also in Dirac materials, such as graphene. One can distinguish between two different strain-induced effects. First, there is a renormalization of the Fermi velocity directly proportional to the local geometric curvature⁷⁸. This space-dependent Fermi velocity is expected to induce spatial oscillations of the local density states near the ripples that are naturally formed in suspended graphene samples⁷⁹. The correlation between the morphology of the

graphene samples and their electronic properties could then explain the local variations of the charge compressibility observed in scanning single electron transistor experiments⁸⁰.

In Dirac materials, in-plane mechanical deformations⁸¹ lead to another curvature-induced effect. Specifically, electrons can react to strain as if external electromagnetic fields were applied. Strain fields indeed result in effective gauge fields [see Box 2] that are opposite in the two graphene valleys. These gauge fields lead to a complete reorganization of the spectrum when they generate a “pseudo”-magnetic field, *i.e.* a magnetic field that is opposite in the two valleys. The latter indeed leads to the appearance of pseudo-Landau levels, and thus represents an important example of strain engineering⁸². Pseudo-Landau levels have been directly imaged using scanning tunneling microscopy in graphene nanobubbles grown on a platinum surface⁸³, as well in flakes supported on nano-pillars⁸⁴. Nanobubbles, in particular, have been shown to generate pseudomagnetic fields as high as 300 T due to the large in-plane strains⁸³. It is important to note that nanobubbles are generally present in van der Waals heterostructures but typically avoided in high-quality devices since in-plane strains represent a dominant factor limiting the electronic mobility⁸⁵. However, nanobubbles have been recently used as active elements for the formation of nanometer-scale lateral p-n junctions in a charge-transfer graphene-based heterostructure⁸⁶.

Strain-induced Landau levels have been also generated in triangular nanoprisms of a SiC substrate [see Fig. 3(b)] and observed by angle-resolved photoemission spectroscopy⁶⁷. A periodic arrangement of pseudomagnetic fields with periods in the tens of nanometer scale [see Fig. 3(c)] has been instead realized in buckled graphene superlattices⁶⁸. The pseudo-Landau levels in this case form weakly dispersive bands that are strongly localized in real space [see Fig. 3(c)]. Since the kinetic energy is quenched, the system can also develop a correlated phase characterized by a pseudogap-like depletion of the density of states, similar to the situation encountered in magic-angle twisted bilayer graphene⁸⁷. Buckling instabilities can be thus exploited to investigate interaction phenomena with important advantages in ease of fabrication and scalability as compared to twistrionics.

C. Quantum nonlinear Hall effect

Strain-induced gauge fields trigger curvature-induced phenomena not strictly related to the presence of pseudo-Landau levels. These occur in non-centrosymmetric materials with Berry curvature: the quantity that encodes the geometric properties associated to the quantum electronic wavefunctions. More specifically, these effects originate from the interplay between the intrinsic crystalline anisotropies of the Dirac material and structural anisotropies induced by certain mechanical deformations. In their pristine form, two-dimensional Dirac materials have a trigonal crystalline structure. Suppose to either induce an highly anisotropic one-dimensional buckling instability or to deposit the nanomembrane onto an anisotropic pre-patterned substrate [see Fig. 3(d)]. The end

product is a superstructured material with an unusually low crystalline symmetry, where all rotational symmetries are broken.

Electronic systems with substantial Berry curvatures and such low-symmetry crystalline content can exhibit a segregation of positive and negative regions of Berry curvature in momentum space leading to a net dipole moment. This Berry curvature dipole yields a quantum nonlinear Hall effect in time-reversal symmetry conditions^{88–90}: a non-linear electro-dynamical phenomenon relevant for high-frequency rectification and long-wavelength photodetection⁹¹. Creating anisotropic mechanical deformations in gated bilayer graphene satisfies all the requirements for the existence of a sizable Berry curvature dipole. Inversion symmetry breaking is achieved with an external electric field perpendicular to the layers. Moreover, anisotropic strains⁷⁰ already in their simplest homogeneous form have been predicted to trigger Berry curvature dipoles [see Fig. 3(d)] comparable to the ones of transition metal dichalcogenides. The observation of a large Berry curvature dipole in corrugated bilayer graphene⁶⁹ has brought to reality the concept of such a curvature-induced quantum nonlinear Hall effect. Importantly, this also opens a new approach to electronic devices that can be used as energy harvesters and terahertz detectors via geometric design.

V. SYNTHESIS AND CHARACTERIZATION METHODS

The creation and exploration of curvature effects strongly relies on the ability to synthesise nanoscale objects with a targeted geometric shape. Curvilinear one-dimensional nano-objects in planar structures can be fabricated using state-of-the-art thin-film technology processing, including electron beam lithography and ion-beam etching. These approaches have been widely used for the fabrication of, for instance, (quantum) rings^{35,40,92}, curved parabolic stripes⁹³, or square loops⁴¹ of different materials. The main advantages of this approach is that the functional curvilinear nanostructure can be easily supplemented with stable electrical contacts for charge injection and gate electrodes. Furthermore, the equilibrium spin textures of magnetic materials can be retrieved using a number of techniques ranging from Lorentz transmission electron microscopy⁹⁴ to X-ray magnetic circular dichroism photoelectron emission (XMCD-PEEM)⁹⁵. Imaging the magnetization states of Ni₈₁Fe₁₉ (permalloy) parabolic stripes using XMCD-PEEM has provided the first experimental evidence of the exchange-driven DMI coupling in curved geometries⁹³. Another advantage of planar structures is that a unique sample can consist of arrays of nano-objects. This configuration is ideal in electronic transport since it naturally provides ensemble averaging that filters out device to device variations^{35,40}. The use of InGaAs square loops arrays⁴¹ for instance has been essential to identify distinctive signatures of the geometric spin-orbit torque in quantum conductance experiments.

The use of planar structures is ideally suited to identify signatures of confinement-induced curvature effects. However, it does not give access to a number of classical shape effects

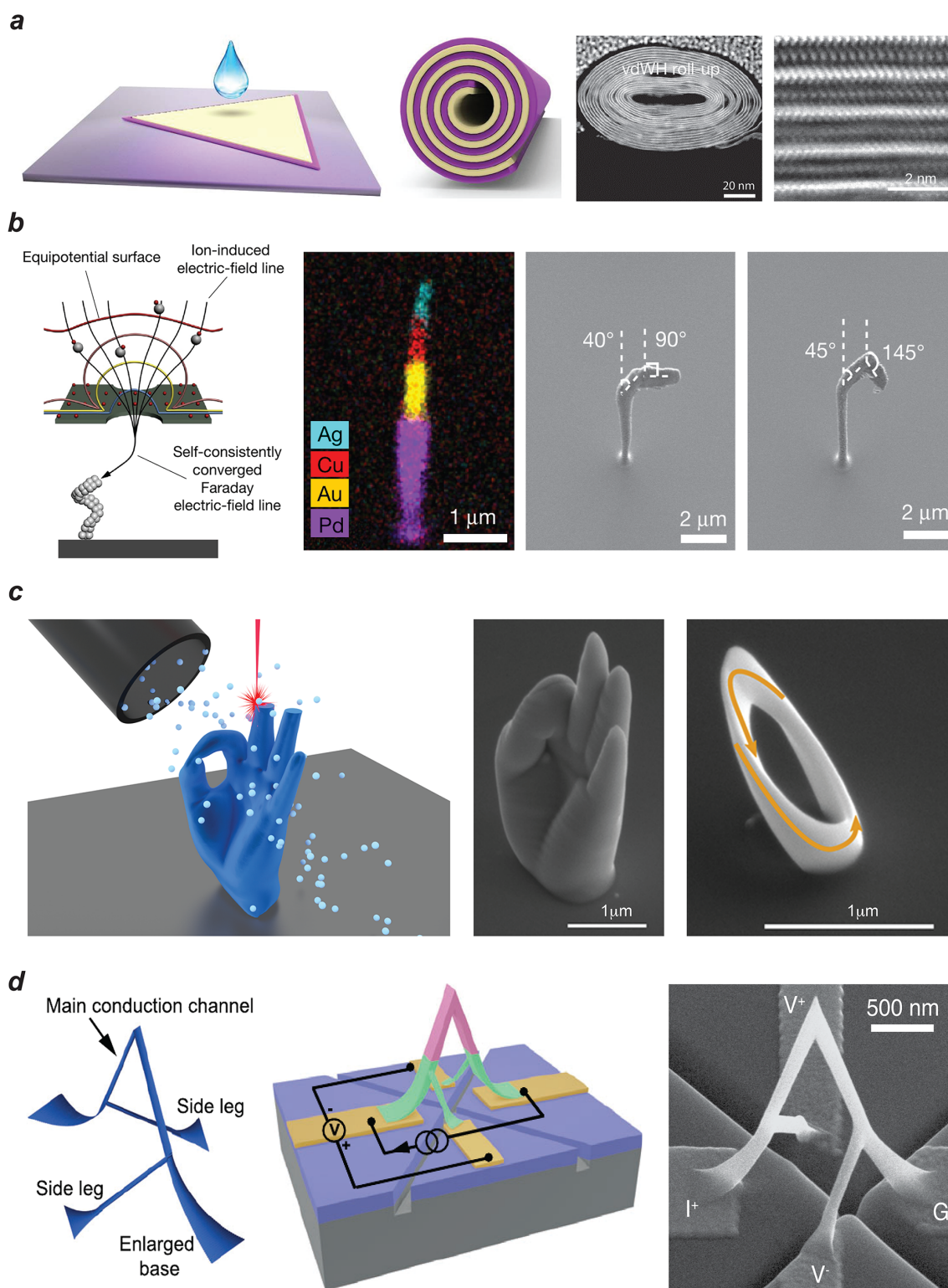


Figure 4. **Fabrication of curvilinear nano-objects.** (a) Schematic illustration of the fabrication process for the formation of high-order rolled up van der Waals heterostructure. The cross-section of the $\text{SnS}_2/\text{WSe}_2$ superlattice was imaged by means of scanning transmission electron microscopy (TEM). Adapted from Ref.⁷. (b) Schematics of nanopillars fabrication by means of charged aerosol particles guided with electrostatic lens and resulting nanopillar formed with various element and geometrical composition imaged by means of scanning electron microscopy (SEM) with energy dispersive X-ray spectroscopy. Adapted from Ref.⁹⁶. (c) Layer-by-layer focused electron beam induced deposition of various self-standing geometries with complex topographies and topologies. Adapted from Ref.⁹⁷. (d) Integration of a ferromagnetic 3D nanobridge in a microelectronic circuit by means of FEBID direct writing technique. Adapted from Ref.⁹⁸.

and strain-driven effects that rely on the synthesis of three-dimensional nanoarchitectures. There are different routes to the fabrication of these complex nanosystems. The first one is based on strain engineering and involves the synthesis at some critical stage of a free-standing nanomembrane released from its substrate by a specialized anisotropic etching procedure⁹⁹. A spatial distribution of strain, engineered in the nanomembrane for instance by heteroepitaxial growth of materials with different lattice constants, then produces a tendency to roll the layer up to create nanotubes¹⁰⁰ or coils¹⁰¹. More elaborate architectures can be formed using additional lithographic patterning. The rolling-up process can be also induced externally. For instance, van der Waals planar heterostructures and monolayers can be driven into a capillary-driven roll-up^{7,102} by inserting or dropping ethanol solution [see Fig.4(a)]. The formation of these nanoarchitectures has led to observe distinctive signatures of shape-driven curvature effects, including the linear transverse magnetoresistance mentioned above. Moreover, compact three-dimensional nanoarchitectures fabricated by rolled-up nanotechnology have footprints orders of magnitude smaller than conventional planar structures. This additional advantage has triggered interest in realizing various functional devices ranging from semiconductor electronic field effect transistors¹⁰³ and high-sensitive sensors for magnetic fields¹⁰⁴, to rolled-up Josephson junctions¹⁰⁵.

The synthesis of three-dimensional nanoarchitectures with complex shapes necessitates other strategies. For example, curved templates such as lithographically patterned substrates, spherical nanoparticles, nanocylinders, or ion-beam induced cones can be coated with a functional material. This generally yields geometric shapes with strongly inhomogeneous thicknesses relevant for shape effects in metallic materials⁶. Patterned substrates can be used to create buckled structures with periodic strain fields that can exist over macroscopic regions⁶⁹. Spherical geometries obtained with the use of silicon-dioxide nanoparticles has allowed to map curvature effects on the magnetic vortex states of magnetic permalloy caps¹⁰⁶. Another method involves the use of pre-stretched elastomeric substrates in which strain relaxation imparts forces at a collection of lithographically patterned locations of precursive planar structures. This results in a process of compressive buckling¹⁰⁷ that extends the structures in the third dimension with broad geometric diversity.

Complex three-dimensional nanosystems can be also fabricated using direct growing and writing methods. Glancing angle deposition, for instance, has been employed to create various functional nanoarchitectures^{108,109}. By tuning the rotation speed of the substrate, vapour source flux intensity and angle of incidence, nano-pillars, nano-flowers and nano-helix arrays have been synthesized. A direct coupling between the chirality of the helices and magnetism¹¹⁰ has been directly proven by the occurrence of magneto-chiral dichroism of light. Recent direct writing techniques include two-photon lithography combined with deposition postprocessing^{111,112}, charged aerogel nanoprining⁹⁶, and focused electron and ion-beam induced depositions^{97,113,114} [see Fig. 4(b),(c)]. Direct writing techniques allow to directly integrate complex three-dimensional architectures into microelectronic circuitry

with lithographically patterned contacts [see Fig. 4(d)]. Using this method, magnetotransport studies of a ferromagnetic three-dimensional nanobridge has brought to light unusual angular dependences in magnetoresistive effects, including the anomalous Hall effect⁹⁸. For three-dimensional nanomagnets a full understanding of curvature-induced effects can be achieved by putting in a one-to-one correspondence the geometric shape with the magnetization distribution. This can be addressed using the recently developed soft X-ray magnetic tomography¹¹⁵ and holographic vector field electron tomography¹¹⁶.

VI. OUTLOOK

These recent advances in the synthesis of three-dimensional nanosystems with complex shapes offer perspectives for the exploration of new geometry-induced nanoscale effects. For example, three-dimensional nanomagnets with a space curve geometry are expected to exhibit a torsion-induced asymmetric spin-wave dispersion⁵⁰ that can be detected using time-resolved scanning transmission X-ray microscopy experiments. When using helimagnetic materials, three-dimensional nano-objects can be also used for the design of magnetoelectric devices. Since the magnetic state can be efficiently controlled by changing the geometry of the wire, embedding the nanomagnet in a piezoelectric matrix allows to achieve an electric-field induced switching between different magnetic states¹¹⁷ that can be assigned logical ‘1’ and ‘0’. Three-dimensional geometries offer means to alter not only intrastructure magnetization textures¹¹⁸ but also offer opportunities to tailor magnetic field nanotextures¹¹⁹. Curvilinear architectures with reconfigurable magnetic field nanotextures are appealing for domain wall-based memory and logic devices: the possibility to pin magnetic domain walls in curvilinear nanowires and to tailor stray field profiles could help optimise the sensor readout of racetrack memories. Moving forward, networks of curvilinear nanowires could be employed for three-dimensional magnonics and related concepts of reservoir computing¹²⁰. Curvilinear antiferromagnets will be instead central in new developments of antiferromagnetic spintronics. Recent theoretical insights promise novel means to control magnetochiral responses, induce weak ferromagnetism and tailor magnonic band gaps¹²¹.

The principle relating strain fields and pseudomagnetic fields in Dirac materials provides a road map to exploit effective gauge fields in nanoelectronics via either spin or pseudospin control¹²². Challenges in the material synthesis are central in this regard. Promising directions are for instance robotic assembly of twisted van der Waals solids¹²³ and controlled formation of nanobubbles via irradiation¹²⁴ or by trapping of substances¹²⁵, in which case curvature radii down to one nm could be achieved¹²⁶. Further progress in the realization of van der Waals rolled-up tubular structures might allow to explore directional-dependent magnetotransport properties intrinsically related to the broken rotational symmetry of a spiralling roll-up. The anisotropy in the transversal magnetoresistance has been predicted¹²⁷ to decrease as $1/w$ with the

number of windings of the roll w , and thus it is practically undetectable in multiple winding nanostructures. Another direction to explore is the design of new material structures for the realization of the classical geometric non-linear Hall effect¹⁵. Because of its very general requirements, this phenomenon can be expected to appear full force also in traditional semiconducting materials where fabrication of high-quality planar curved channels can be achieved.

A frontier in the field is to individuate electronic fingerprints of the quantum geometric potential, as its existence has been verified so far only in metamaterials¹²⁸. In thin films with inhomogeneous curvature profile, the quantum geometric potential results in an in-plane internal electric field. This built-in electric field can potentially drive a linear Hall-like effect at zero magnetic field in materials with substantial Berry curvature such as transition metal dichalcogenides. This Magnus Hall effect¹²⁹ could therefore provide the very first experimental confirmation of the existence of the quantum geometric potential. The role of geometry in the family of Hall effects is expected to become even more relevant when reaching the quantum Hall regime. In (synthetic) material structures with locally non-flat geometries, the electronic density of a quantum Hall fluid is directly coupled to the Gaussian curvature via the so-called mean orbital spin¹³⁰. Furthermore, additionally designing lattice disclinations would lead to an intrinsic rotation of the electronic fluid caused by gravitational anomalies¹³¹. Synthesis of electronic nanomembranes with engineered nanodomains of substantial Gaussian curvature represent a promising path to bring this concept to reality. This would allow for an entirely new generation of tabletop experiments where concepts of elasticity, topology and cosmology are intertwined. Such crucial experimental efforts will also rely on new theoretical directions to understand how to disentangle physical phenomena related to confinement-induced curvature effects and geometric transport effects.

Additional evidence of the interplay between the real-space geometry of a nanosystem and the internal geometry of the electronic wavefunctions, first unveiled in corrugated bilayer graphene⁶⁹, could be pursued in complex oxides such as SrRuO₃. Ultrathin films of this magnetic material are characterized by strong Berry curvature¹³². Moreover, monocrystalline nanomembranes have been isolated¹³³ and could be transferred to curved templates. Periodically curved layers of this material have been also obtained starting out from a ferroelectric-metal superlattice¹³⁴. Oxide electronic devices thus represent an ideal material platform to explore nanoscale geometry effects in quantum phenomena. The use of nanoscale curvature for the synthesis of superstructures with reduced crystalline symmetry content is likely to play a vital role in the search for unconventional superconducting phases, including orbital combinations of pair density waves¹³⁵, which could be relevant for superconducting orbitronics. Crucial will be also efforts in using nanoscale geometry-induced effects to design more resilient topological superconducting phases¹³⁶ or even turn a "conventional" superconductor into a topological one. We envision that developments in this direction could result in new paradigms for topological superconducting circuitry.

The recent advances, which we have reviewed, together with the new opportunities and challenges mentioned above indicate curved electronics as a nascent and rich subject of research relevant for fundamental physics and device engineering.

VII. BOX 1: ORIGIN OF CONFINEMENT-INDUCED CURVATURE EFFECTS

Let us first illustrate the emergence of curvature effects resulting from the quantum dynamics of charge carriers in the non-relativistic regime. Consider an electron entering a curved channel. For its mean trajectory to follow the geometry of the structure, the electron must be subject to an usual (harmonic) confining potential with the addition of an electric field directed along the normal that forces its mean velocity to change direction. Clearly, the strength of this electric field grows linearly with the local curvature of the channel. To monitor its effect, it is possible to employ an adiabatic separation between fast and slow quantum degrees of freedom. In particular, the quantum motion in the strongly confined fast normal direction can be obtained by solving at each tangential position a one-dimensional Schrödinger equation. Due to the presence of the electric field, the energy levels depart from those of the quantum harmonic potential. This deviation is of the second-order since the first-order correction vanishes by symmetry. The local energy correction is thus negative and builds up an attractive potential for the slow degrees of freedom $\propto \hbar^2 \kappa(s)^2 / m^*$ with $\kappa(s)$ the local geometric curvature and m^* the electronic effective mass. The existence of this quantum geometric potential has been rigorously proved by Jensen, Koppe¹³⁷ and Da Costa¹³⁸ by employing a thin-wall quantization procedure. It starts with the Schrödinger equation in a generic curved portion of space embedding the surface or line of interest. The latter can be written as $-\hbar^2 G^{ij} \mathcal{D}_i \mathcal{D}_j \psi = 2m^* E \psi$ where one introduces the covariant derivative of a generic vector field \mathbf{v} as

$$\mathcal{D}_i v_j = \partial_i v_j - \Gamma_{ij}^k v_k,$$

with Γ_{ij}^k being the antisymmetric Christoffel symbols. The connection and the metric tensor G_{ij} can be related to the geometric properties of the lower-dimensional manifold assuming the quantum particle is strongly confined in the normal direction. Moreover, it is possible to safely take a zero thickness limit once a rescaled wavefunction with a well-defined surface density probability is introduced. The end product is a dimensionally-reduced Schrödinger equation for a free particle but with the addition of the quantum geometric potential

$$\mathcal{V}_g = -\frac{\hbar^2}{2m^*} (M^2 - K),$$

where M is the mean curvature and K is the gaussian curvature of the generic bent surface. For the case of one-dimensional curves with a single principal curvature $\kappa(s)$ the geometric potential reduces to $-\hbar^2 \kappa(s)^2 / (8m^*)$ in agreement with the qualitative argument given above.

Materials with sizable spin-orbit coupling possess additional geometry-induced effects. Consider for instance a curvilinear one-dimensional nanostructure. Its low-energy effective Rashba spin-orbit coupled Hamiltonian can be written as

$$\mathcal{H} = -\frac{\hbar^2}{2m^*} \partial_s^2 + \frac{i\hbar\alpha}{2} [\sigma_N(s)\partial_s + \partial_s\sigma_N(s)],$$

where α is the Rashba spin-orbit coupling strength and we introduced the triad of Pauli matrices $\{\sigma_T, \sigma_N, \sigma_B\}$ comoving with the curvilinear Frenet-Serret frame determined by the tangential, normal, and binormal directions¹³⁹. By completing the square in the Hamiltonian, it is possible to show that the expectation values of the spin component are determined by a local operator $\hat{G}(s) = -\sigma_N(s)/(2l_\alpha) - \beta\sigma_0$ where $l_\alpha = \hbar/(2m^*\alpha)$ is the spin-orbit interaction length while β is a constant that depends on the eigen-energy and does not affect the spin textures. By further using the commutation relations for the triad of Frenet-Serret of Pauli matrices, one finds an equation that links the electron spin orientation in the Frenet-Serret frame, the strength of the Rashba spin-orbit interaction and the geometric curvature. This fundamental equation³⁶ reads

$$\partial_s \langle \boldsymbol{\sigma} \rangle = -\mathbf{h}_{eff} \times \langle \boldsymbol{\sigma} \rangle,$$

where the effective field lies in the normal-binormal plane and has an explicit geometric component given by the local curvature $\kappa(s)$ since $\mathbf{h}_{eff} = \{0, l_\alpha^{-1}, \kappa(s)\}$. For non-zero curvature the electron spin acquires a finite out-of-plane binormal component. Additionally, and as discussed in the main text, for inhomogeneous curvature there is a finite torque that yields an unconventional tangential spin component. This curvature control of the spin textures is reflected in the real-space geometry control of a quantum geometric phase. There is in fact a direct relation linking the spin texture to the Aharonov-Anandan (AA) geometric phase. We recall that the AA phase is the non-adiabatic analog of the Berry phase which can be defined as $\gamma = \oint_{\mathcal{C}} d\mathbf{r} \cdot \mathcal{A}$, with \mathcal{A} the Berry connection $\mathcal{A} = -i \langle \boldsymbol{\psi}(\mathbf{r}) | \nabla | \boldsymbol{\psi}(\mathbf{r}) \rangle$. The Berry curvature is the field strength with components $\Omega_{r_a} = \varepsilon_{abc} \partial_{r_b} \mathcal{A}_{r_c}$ and transforms as a pseudovector in three-dimensions, and as a pseudoscalar in two-dimensional systems.

In ferromagnetic materials, confinement effects on the exchange magnetic energy yield a curvature-induced Dzyaloshinskii-Moriya interaction (DMI) and a magnetic anisotropy. Precisely as for the quantum geometric potential, one starts with the exchange energy in a thin curved shell with the energy density written as usual $\mathcal{E}_{ex} = \nabla \mathbf{m} \cdot \nabla \mathbf{m}$, where \mathbf{m} is the magnetization. The zero-thickness limit of this three-dimensional exchange magnetic energy yields a surface energy consisting of three-different terms¹⁴⁰, *i.e.* $\mathcal{E}_{ex} = \mathcal{E}_{ex}^0 + \mathcal{E}_{ex}^D + \mathcal{E}_{ex}^A$. For a generic curved surface and assuming an orthonormal curvilinear local basis has been found, the three

different contributions can be written as follows

$$\begin{aligned} \mathcal{E}_{ex}^0 &= \nabla_\alpha m_\beta \nabla_\alpha m_\beta + \nabla_\alpha m_n \nabla_\alpha m_n \\ \mathcal{E}_{ex}^D &= 2h_{\alpha\beta} (m_\beta \nabla_\alpha m_n - m_n \nabla_\alpha m_\beta) + 2\varepsilon_{\alpha\beta} \Omega_\gamma m_\beta \nabla_\gamma m_\alpha \\ \mathcal{E}_{ex}^A &= (h_{\alpha\gamma} h_{\gamma\beta} + \Omega^2 \delta_{\alpha\beta}) m_\alpha m_\beta + (M^2 - 2K) m_n^2 + \\ &\quad 2\varepsilon_{\alpha\gamma} h_{\gamma\beta} \Omega_\beta m_\alpha m_n. \end{aligned}$$

In the equation above, we introduced the Weingarten curvature tensor $h_{\alpha\beta}$, the spin connection Ω associated of the two-dimensional curved surface, and the two-dimensional Levi-Civita tensor $\varepsilon_{\alpha\beta}$. Additionally, m_n is the component of the magnetization in the direction normal to the curved surface. The emergence of the curvature-induced DMI interaction, in particular, reflects the fact that bending of a curved thin magnetic layer breaks the centrosymmetry.

In superconductors, an homogeneous spin-triplet pairing order parameter can be conveniently expressed introducing the so-called \mathbf{d} -vector:

$$\hat{\Delta} = \begin{pmatrix} \Delta^{\uparrow\uparrow} & \Delta^{\uparrow\downarrow} \\ \Delta^{\uparrow\downarrow} & \Delta^{\downarrow\downarrow} \end{pmatrix} \equiv i(\mathbf{d} \cdot \boldsymbol{\sigma})_y,$$

where we used the relation $\Delta^{\uparrow\downarrow} = \Delta^{\downarrow\uparrow}$. The complex components of \mathbf{d} -vector are related to the pair amplitudes by

$$\mathbf{d} = \left(-\frac{\Delta^{\uparrow\uparrow} - \Delta^{\downarrow\downarrow}}{2}, \frac{\Delta^{\uparrow\uparrow} + \Delta^{\downarrow\downarrow}}{2i}, \Delta^{\uparrow\downarrow} \right).$$

Hence, each component of the \mathbf{d} -vector indicates the pair amplitude for the Cooper-pair spin perpendicular to the corresponding spin axis. Non-vanishing amplitudes of the \mathbf{d} -vector components are mainly dictated by the structure of the pairing potential while the orientation of the \mathbf{d} -vector is determined, for instance, by spin-orbit coupling, magnetic fields or intrinsic magnetism. Triplet pairing with a non-zero value of the product $\mathbf{d} \times \mathbf{d}^*$ implies that the spins of the Cooper pairs are polarized. Additionally, the relative 0 (π) spin-phase difference appearing between the $\Delta^{\uparrow\uparrow}$ and $\Delta^{\downarrow\downarrow}$ matrix elements when only the d_y (d_x) component is present, can be relevant for superconducting spintronic applications. One can generally show that there will be a non-trivial Josephson coupling, both in the charge and spin channel, which depends on the relative \mathbf{d} -vector misalignment angle. For the case of a typical Josephson junction configuration with tunnel coupled superconducting regions marked by \mathbf{d} -vectors with a misalignment angle β , the Josephson current¹⁴¹ for the charge and spin sector is proportional to $[\sin(\phi + \beta) + \sin(\phi - \beta)]$ and $[\sin(\phi + \beta) - \sin(\phi - \beta)]$ respectively, with ϕ being the phase difference between the \mathbf{d} -vectors.

VIII. BOX 2: GAUGE FIELDS IN STRAINED NANOSTRUCTURES

We illustrate the emergence of gauge fields in strained nanosystem with Dirac electrons by considering the specific example of graphene, and start with the simplest tight-binding

model Hamiltonian, *i.e.* considering only hopping processes between nearest neighbor atomic sites, which reads

$$\mathcal{H}_{MLG} = - \sum_{in} t_n a_i^\dagger b_{i+\delta_n} + c.c.,$$

where a^\dagger and b^\dagger (a, b) are creation (annihilation) operators on the A and B sublattices respectively. In the equation above, the subscript i runs over all unit cell positions, and we introduced the three nearest neighbor vectors

$$\delta_1 = \frac{a}{\sqrt{3}} \left\{ \frac{\sqrt{3}}{2}, \frac{1}{2} \right\}; \delta_2 = \frac{a}{\sqrt{3}} \left\{ \frac{-\sqrt{3}}{2}, \frac{1}{2} \right\}; \delta_3 = \frac{a}{\sqrt{3}} \{0, -1\}.$$

The presence of strain implies that the hopping amplitudes t_n explicitly depend on the nearest neighbor vectors. Specifically, $t_n = t_0 (1 - \beta \delta u_n)$ where t_0 is the hopping amplitude for the pristine threefold rotation symmetric honeycomb lattice, the lattice parameter β can be determined by Raman spectroscopy whereas the relative distance changes δu_n can be expressed in terms of the strain tensor components ϵ_{ij} as

$$\delta u_n = \frac{\delta_n^i \delta_n^j}{a^2} \epsilon_{ij}.$$

To proceed further, we go to momentum space and write the Bloch Hamiltonian as

$$\mathcal{H}_{MLG} = - \sum_n t_n \begin{pmatrix} 0 & e^{-i(\mathbf{K}^{(l)} + \mathbf{q}) \cdot \delta_n} \\ e^{i(\mathbf{K}^{(l)} + \mathbf{q}) \cdot \delta_n} & 0 \end{pmatrix},$$

where we have rewritten the momenta as $\mathbf{k} = \mathbf{K}^{(l)} + \mathbf{q}$ since we are interested in the electronic properties close to the \mathbf{K} or \mathbf{K}' valleys of the Brillouin zone (BZ) given by $\mathbf{K} = \left\{ \frac{4\pi}{3\sqrt{3}a}, 0 \right\}$

and $\mathbf{K}' = \left\{ -\frac{4\pi}{3\sqrt{3}a}, 0 \right\}$. The Bloch Hamiltonian can be then expanded to linear order in the small momenta q . Using simple vector identities and assuming for simplicity an anisotropic biaxial strain with $\epsilon_{xx} \neq \epsilon_{yy} \neq 0$ and $\epsilon_{xy} \equiv 0$ the continuum low-energy Hamiltonian near the two valleys of the BZ can be then recast as

$$\mathcal{H}_{eff}(\mathbf{q}) = \xi v_x q_x \sigma_x + v_F \mathcal{A}_x \sigma_x + v_y q_y \sigma_y$$

where $\xi = \pm 1$ is the valley index. Here $\mathcal{A}_x = \sqrt{3} \beta (\epsilon_{xx} - \epsilon_{yy}) / (2a)$ is a strain-induced ‘‘pseudo’’-gauge field whereas $v_F = \sqrt{3} t_0 a / 2$ is the Fermi velocity of the Dirac carriers in unstrained samples. In addition, $v_x = v_F [1 - \beta (3\epsilon_{xx} + \epsilon_{yy}) / 4]$ and $v_y = v_F [1 - \beta (\epsilon_{xx} + 3\epsilon_{yy}) / 4]$ are renormalized Fermi velocities that become anisotropic due to momentum-strain coupling.

Acknowledgements: We would like to acknowledge the numerous colleagues with whom we have collaborated on the topics described in this Review. We would also like to acknowledge the Future and Emerging Technologies (FET) Programme within the Seventh Framework Programme for Research of the European Commission under FET-Open Grant No.618083 (CNTQC) for the financial support to the work performed by the authors on this topic. C.O. acknowledges support from a VIDI grant (Project 680-47-543) financed by the Netherlands Organization for Scientific Research (NWO). The work of D.M. and O.M.V. was financed in part via numerous national and European projects including German Research Foundation (DFG) Grants MA 5144/9-1, MA 5144/13-1, MA 5144/28-1, VO 2598/1-1, and Helmholtz Association of German Research Centres in the frame of the Helmholtz Innovation Lab ‘‘FlexiSens’’. Z.-J. Y. acknowledges support from the National Natural Science Foundation of China (Grant No. 11974151).

Author Contributions: C.O. coordinated the project. P.G. produced the original illustrations. All authors wrote and commented on the manuscript.

- ¹ Stuart S. P. Parkin, Masamitsu Hayashi, and Luc Thomas, ‘‘Magnetic domain-wall racetrack memory,’’ *Science* **320**, 190–194 (2008).
- ² Manfred Albrecht, Guohan Hu, Ildico L. Guhr, Till C. Ulbrich, Johannes Boneberg, Paul Leiderer, and Günter Schatz, ‘‘Magnetic multilayers on nanospheres,’’ *Nature Materials* **4**, 203–206 (2005).
- ³ Reinoud Lavrijsen, Ji-Hyun Lee, Amalio Fernández-Pacheco, Dorothée C. M. C. Petit, Rhodri Mansell, and Russell P. Cowburn, ‘‘Magnetic ratchet for three-dimensional spintronic memory and logic,’’ *Nature* **493**, 647–650 (2013).
- ⁴ Christian Becker, Daniil Karnaushenko, Tong Kang, Dmitriy D. Karnaushenko, Maryam Faghih, Alaleh Mirhajivarzaneh, and Oliver G. Schmidt, ‘‘Self-assembly of highly sensitive 3d magnetic field vector angular encoders,’’ *Science Advances* **5**, eaay7459 (2019).
- ⁵ Daniil Karnaushenko, Dmitriy D. Karnaushenko, Denys Makarov, Stefan Baunack, Rudolf Schäfer, and Oliver G.

Schmidt, ‘‘Self-assembled on-chip-integrated giant magneto-impedance sensorics,’’ *Advanced Materials* **27**, 6582–6589 (2015).

- ⁶ K. S. Das, D. Makarov, P. Gentile, M. Cuoco, B. J. van Wees, C. Ortix, and I. J. Vera-Marun, ‘‘Independent geometrical control of spin and charge resistances in curved spintronics,’’ *Nano Letters* **19**, 6839–6844 (2019).
- ⁷ B. Zhao, Z. Wan, Y. Liu, J. Xu, X. Yang, D. Shen, Z. Zhang, C. Guo, Q. Qian, J. Li, R. Wu, Z. Lin, X. Yan, B. Li, Z. Zhang, H. Ma, B. Li, X. Chen, Y. Qiao, I. Shakir, Z. Almutairi, F. Wei, Y. Zhang, X. Pan and Y. Huang, Y. Ping, X. Duan, and X. Duan, ‘‘High-order superlattices by rolling up van der waals heterostructures,’’ *Nature* **591**, 385–390 (2021).
- ⁸ Ching-Hao Chang and Carmine Ortix, ‘‘Theoretical prediction of a giant anisotropic magnetoresistance in carbon nanoscrolls,’’ *Nano Letters*, *Nano Letters* **17**, 3076–3080 (2017).
- ⁹ Werner Steinhögl, Günther Schindler, Gernot Steinlesberger, and Manfred Engelhardt, ‘‘Size-dependent resistivity of metallic

- wires in the mesoscopic range,” *Phys. Rev. B* **66**, 075414 (2002).
- 10 F. J. Jedema, A. T. Filip, and B. J. van Wees, “Electrical spin injection and accumulation at room temperature in an all-metal mesoscopic spin valve,” *Nature* **410**, 345–348 (2001).
 - 11 S. O. Valenzuela and M. Tinkham, “Spin-polarized tunneling in room-temperature mesoscopic spin valves,” *Applied Physics Letters* **85**, 5914–5916 (2004).
 - 12 T. Kimura and Y. Otani, “Large spin accumulation in a permalloy-silver lateral spin valve,” *Phys. Rev. Lett.* **99**, 196604 (2007).
 - 13 Igor Žutić, Jaroslav Fabian, and S. Das Sarma, “Spintronics: Fundamentals and applications,” *Rev. Mod. Phys.* **76**, 323–410 (2004).
 - 14 T. Kimura, T. Sato, and Y. Otani, “Temperature evolution of spin relaxation in a NiFe/Cu lateral spin valve,” *Phys. Rev. Lett.* **100**, 066602 (2008).
 - 15 Nicholas B. Schade, David I. Schuster, and Sidney R. Nagel, “A nonlinear, geometric hall effect without magnetic field,” *Proceedings of the National Academy of Sciences* **116**, 24475–24479 (2019).
 - 16 M. S. Dresselhaus, Gene Dresselhaus, and Phaedon Avouris, *Carbon Nanotubes: Synthesis, Structure, Properties, and Applications*, 1st ed. (Springer-Verlag Berlin Heidelberg, 2001).
 - 17 Sagar Bhandari, Gil-Ho Lee, Anna Klates, Kenji Watanabe, Takashi Taniguchi, Eric Heller, Philip Kim, and Robert M. Westervelt, “Imaging cyclotron orbits of electrons in graphene,” *Nano Letters* **16**, 1690–1694 (2016).
 - 18 S. N. Song, X. K. Wang, R. P. H. Chang, and J. B. Ketterson, “Electronic properties of graphite nanotubules from galvanomagnetic effects,” *Phys. Rev. Lett.* **72**, 697–700 (1994).
 - 19 A. Yu. Kasumov, I. I. Khodos, P. M. Ajayan, and C. Colliex, “Electrical resistance of a single carbon nanotube,” *EPL (Europhysics Letters)* **34**, 429 (1996).
 - 20 Alessandro Cresti, Michael M. Fogler, Francisco Guinea, A. H. Castro Neto, and Stephan Roche, “Quenching of the quantum hall effect in graphene with scrolled edges,” *Phys. Rev. Lett.* **108**, 166602 (2012).
 - 21 J. E. Müller, “Effect of a nonuniform magnetic field on a two-dimensional electron gas in the ballistic regime,” *Phys. Rev. Lett.* **68**, 385–388 (1992).
 - 22 Lisa M. Viculis, Julia J. Mack, and Richard B. Kaner, “A chemical route to carbon nanoscrolls,” *Science* **299**, 1361–1361 (2003).
 - 23 Xu Xie, Long Ju, Xiaofeng Feng, Yinghui Sun, Ruifeng Zhou, Kai Liu, Shoushan Fan, Qunqing Li, and Kaili Jiang, “Controlled fabrication of high-quality carbon nanoscrolls from monolayer graphene,” *Nano Letters* **9**, 2565–2570 (2009).
 - 24 Kostiantyn V. Yershov, Volodymyr P. Kravchuk, Denis D. Sheka, and Ulrich K. Rössler, “Curvature effects on phase transitions in chiral magnets,” *SciPost Phys.* **9**, 43 (2020).
 - 25 Lincoln J. Lauhon, Mark S. Gudiksen, Deli Wang, and Charles M. Lieber, “Epitaxial core-shell and core-multishell nanowire heterostructures,” *Nature* **420**, 57–61 (2002).
 - 26 Torsten Rieger, Martina Luysberg, Thomas Schäpers, Detlev Grützmacher, and Mihail Ion Lepsa, “Molecular beam epitaxy growth of gaas/inas core-shell nanowires and fabrication of inas nanotubes,” *Nano Letters*, *Nano Letters* **12**, 5559–5564 (2012).
 - 27 Tomas Orn Rosdahl, Andrei Manolescu, and Vidar Gudmundsson, “Signature of snaking states in the conductance of core-shell nanowires,” *Nano Letters* **15**, 254–258 (2015).
 - 28 Peter Rickhaus, Péter Makk, Ming-Hao Liu, Endre Tóvári, Markus Weiss, Romain Maurand, Klaus Richter, and Christian Schönenberger, “Snake trajectories in ultraclean graphene p–n junctions,” *Nature Communications* **6**, 6470 (2015).
 - 29 Thiti Taychatanapat, Jun You Tan, Yuting Yeo, Kenji Watanabe, Takashi Taniguchi, and Barbaros Özyilmaz, “Conductance oscillations induced by ballistic snake states in a graphene heterojunction,” *Nature Communications* **6**, 6093 (2015).
 - 30 Giulio Ferrari, Guido Goldoni, Andrea Bertoni, Giampaolo Cuoghi, and Elisa Molinari, “Magnetic states in prismatic core multishell nanowires,” *Nano Letters*, *Nano Letters* **9**, 1631–1635 (2009).
 - 31 Jens H. Bardarson and Joole E. Moore, “Quantum interference and aharonov bohm oscillations in topological insulators,” *Reports on Progress in Physics* **76**, 056501 (2013).
 - 32 J. Dufouleur, L. Veyrat, A. Teichgräber, S. Neuhaus, C. Nowka, S. Hampel, J. Cayssol, J. Schumann, B. Eichler, O. G. Schmidt, B. Büchner, and R. Giraud, “Quasiballistic transport of dirac fermions in a bi_2se_3 nanowire,” *Phys. Rev. Lett.* **110**, 186806 (2013).
 - 33 J. Ziegler, R. Kozlovsky, C. Gorini, M.-H. Liu, S. Weishäupl, H. Maier, R. Fischer, D. A. Kozlov, Z. D. Kvon, N. Mikhailov, S. A. Dvoretzky, K. Richter, and D. Weiss, “Probing spin helical surface states in topological hgte nanowires,” *Phys. Rev. B* **97**, 035157 (2018).
 - 34 Raphael Kozlovsky, Ansgar Graf, Denis Kochan, Klaus Richter, and Cosimo Gorini, “Magnetoconductance, quantum hall effect, and coulomb blockade in topological insulator nanocones,” *Phys. Rev. Lett.* **124**, 126804 (2020).
 - 35 Fumiya Nagasawa, Diego Frustaglia, Henri Saarikoski, Klaus Richter, and Junsaku Nitta, “Control of the spin geometric phase in semiconductor quantum rings,” *Nature Communications* **4**, 2526 (2013).
 - 36 Zu-Jian Ying, Paola Gentile, Carmine Ortix, and Mario Cuoco, “Designing electron spin textures and spin interferometers by shape deformations,” *Phys. Rev. B* **94**, 081406 (2016).
 - 37 Junsaku Nitta, Frank E. Meijer, and Hideaki Takayanagi, “Spin-interference device,” *Applied Physics Letters* **75**, 695–697 (1999).
 - 38 M. König, A. Tschetschetkin, E. M. Hankiewicz, Jairo Sinova, V. Hock, V. Daumer, M. Schäfer, C. R. Becker, H. Buhmann, and L. W. Molenkamp, “Direct observation of the aharonov-casher phase,” *Phys. Rev. Lett.* **96**, 076804 (2006).
 - 39 Diego Frustaglia and Klaus Richter, “Spin interference effects in ring conductors subject to rashba coupling,” *Phys. Rev. B* **69**, 235310 (2004).
 - 40 Fumiya Nagasawa, Jun Takagi, Yoji Kunihashi, Makoto Kohda, and Junsaku Nitta, “Experimental demonstration of spin geometric phase: Radius dependence of time-reversal aharonov-casher oscillations,” *Phys. Rev. Lett.* **108**, 086801 (2012).
 - 41 M. Wang, H. Saarikoski, A. A. Reynoso, J. P. Baltanás, D. Frustaglia, and J. Nitta, “Geometry-assisted topological transitions in spin interferometry,” *Phys. Rev. Lett.* **123**, 266804 (2019).
 - 42 Paola Gentile, Mario Cuoco, and Carmine Ortix, “Edge states and topological insulating phases generated by curving a nanowire with rashba spin-orbit coupling,” *Phys. Rev. Lett.* **115**, 256801 (2015).
 - 43 J. Zak, “Symmetry criterion for surface states in solids,” *Phys. Rev. B* **32**, 2218–2226 (1985).
 - 44 Sudhakar Pandey, Niccolò Scopigno, Paola Gentile, Mario Cuoco, and Carmine Ortix, “Topological quantum pump in serpentine-shaped semiconducting narrow channels,” *Phys. Rev. B* **97**, 241103 (2018).
 - 45 D. J. Thouless, “Quantization of particle transport,” *Phys. Rev. B* **27**, 6083–6087 (1983).
 - 46 Q. Niu, “Towards a quantum pump of electric charges,” *Phys. Rev. Lett.* **64**, 1812–1815 (1990).

- ⁴⁷ Oleksandr V. Pylypovskiy, Denis D. Sheka, Volodymyr P. Kravchuk, Kostiantyn V. Yershov, Denys Makarov, and Yuri Gaididei, “Rashba torque driven domain wall motion in magnetic helices,” *Scientific Reports* **6**, 23316 (2016).
- ⁴⁸ Kostiantyn V. Yershov, Volodymyr P. Kravchuk, Denis D. Sheka, and Yuri Gaididei, “Curvature and torsion effects in spin-current driven domain wall motion,” *Phys. Rev. B* **93**, 094418 (2016).
- ⁴⁹ Yuri Gaididei, Volodymyr P. Kravchuk, and Denis D. Sheka, “Curvature effects in thin magnetic shells,” *Phys. Rev. Lett.* **112**, 257203 (2014).
- ⁵⁰ Denis D. Sheka, Volodymyr P. Kravchuk, Kostiantyn V. Yershov, and Yuri Gaididei, “Torsion-induced effects in magnetic nanowires,” *Phys. Rev. B* **92**, 054417 (2015).
- ⁵¹ A. Bogdanov and A. Hubert, “Thermodynamically stable magnetic vortex states in magnetic crystals,” *Journal of Magnetism and Magnetic Materials* **138**, 255–269 (1994).
- ⁵² Xiaohong Huo and Yan Liu, “The stability of a skyrmion in a nanotube,” *New Journal of Physics* **21**, 093024 (2019).
- ⁵³ Ming Yan, Christian Andreas, Attila Kakay, Felipe Garcia-Sanchez, and Riccardo Hertel, “Chiral symmetry breaking and pair-creation mediated walker breakdown in magnetic nanotubes,” *Applied Physics Letters* **100**, 252401 (2012).
- ⁵⁴ N. L. Schryer and L. R. Walker, “The motion of 180° domain walls in uniform dc magnetic fields,” *Journal of Applied Physics* **45**, 5406–5421 (1974).
- ⁵⁵ Jorge A. Otálora, Ming Yan, Helmut Schultheiss, Riccardo Hertel, and Attila Kákay, “Curvature-induced asymmetric spin-wave dispersion,” *Phys. Rev. Lett.* **117**, 227203 (2016).
- ⁵⁶ Lukas Körber, Michael Zimmermann, Sebastian Wintz, Simone Finizio, Matthias Kronseder, Dominique Bougeard, Florian Dirnberger, Markus Weigand, Jörg Raabe, Jorge A. Otálora, Helmut Schultheiss, Elisabeth Josten, Jürgen Lindner, Istvan Kezmarki, Christian H. Back, and Attila Kakay, “Symmetry- and curvature effects on spin waves in vortex-state hexagonal nanotubes,” (2021), [arXiv:2108.07103 \[cond-mat.mes-hall\]](https://arxiv.org/abs/2108.07103).
- ⁵⁷ M. Linder and J. W. A. Robinson, “Superconducting spintronics,” *Nature Physics* **11**, 307 (2015).
- ⁵⁸ M. Sigrist and K. Ueda, “Phenomenological theory of unconventional superconductivity,” *Review of Modern Physics* **63**, 239 (1991).
- ⁵⁹ F. S. Bergeret, A. F. Volkov, and K. B. Efetov, “Long-range proximity effects in superconductor-ferromagnet structures,” *Phys. Rev. Lett.* **86**, 4096–4099 (2001).
- ⁶⁰ M. Eschrig and T. Löfwander, “Triplet supercurrents in clean and disordered half-metallic ferromagnets,” *Nature Physics* **4**, 138–143 (2008).
- ⁶¹ J. W. A. Robinson, J. D. S. Witt, and M.G. Blamire, “Controlled injection of spin-triplet supercurrents into a strong ferromagnet,” *Science* **329**, 59 (2010).
- ⁶² F. S. Bergeret and I. V. Tokatly, “Spin-orbit coupling as a source of long-range triplet proximity effect in superconductor-ferromagnet hybrid structures,” *Phys. Rev. B* **89**, 134517 (2014).
- ⁶³ Lev P. Gorkov and Emmanuel I. Rashba, “Superconducting 2d system with lifted spin degeneracy: Mixed singlet-triplet state,” *Phys. Rev. Lett.* **87**, 037004 (2001).
- ⁶⁴ P. A. Frigeri, D. F. Agterberg, A. Koga, and M. Sigrist, “Superconductivity without inversion symmetry: Mnsi versus cept₃si,” *Physical Review Letters* **92**, 097001 (2004).
- ⁶⁵ Zu-Jian Ying, Mario Cuoco, Carmine Ortix, and Paola Gentile, “Tuning pairing amplitude and spin-triplet texture by curving superconducting nanostructures,” *Physical Review B* **96**, 100506(R) (2017).
- ⁶⁶ Gianluca Francica, Mario Cuoco, and Paola Gentile, “Topological superconducting phases and josephson effect in curved superconductors with time reversal invariance,” *Physical Review B* **96**, 100506(R) (2017).
- ⁶⁷ P. Nigge, A. C. Qu, E. Lantagne-Hurtubise, E. Marsell, S. Link, G. Tom, M. Zonno, M. Michiardi, M. Schneider, S. Zhdanovich, G. Levy, U. Starke, C. Gutierrez, D. Bonn, S. A. Burke, M. Franz, and A. Damascelli, “Room temperature strain-induced landau levels in graphene on a wafer-scale platform,” *Science Advances* **5**, eaaw5593 (2019).
- ⁶⁸ Jinhai Mao, Slavisa P. Milovanović, Misa Anđelković, Xinyuan Lai, Yang Cao, Kenji Watanabe, Takashi Taniguchi, Lucian Covaci, Francois M. Peeters, Andre K. Geim, Yuhang Jiang, and Eva Y. Andrei, “Evidence of flat bands and correlated states in buckled graphene superlattices,” *Nature* **584**, 215–220 (2020).
- ⁶⁹ Sheng-Chin Ho, Ching-Hao Chang, Yu-Chiang Hsieh, Shun-Tsung Lo, Botsz Huang, Thi-Hai-Yen Vu, Carmine Ortix, and Tse-Ming Chen, “Hall effects in artificially corrugated bilayer graphene without breaking time-reversal symmetry,” *Nature Electronics* **4**, 116–125 (2021).
- ⁷⁰ Raffaele Battilomo, Niccolò Scopigno, and Carmine Ortix, “Berry curvature dipole in strained graphene: A fermi surface warping effect,” *Phys. Rev. Lett.* **123**, 196403 (2019).
- ⁷¹ Yongfeng Mei, Suwit Kiravittaya, Mohamed Benyoucef, Dominic J. Thurmer, Tim Zander, Christoph Deneke, Francesca Cavallo, Armando Rastelli, and Oliver G. Schmidt, “Optical properties of a wrinkled nanomembrane with embedded quantum well,” *Nano Letters* **7**, 1676–1679 (2007).
- ⁷² Pavlo Zubko, Gustau Catalan, and Alexander K. Tagantsev, “Flexoelectric effect in solids,” *Annual Review of Materials Research* **43**, 387–421 (2013).
- ⁷³ Chris G. Van de Walle, “Band lineups and deformation potentials in the model-solid theory,” *Phys. Rev. B* **39**, 1871–1883 (1989).
- ⁷⁴ Carmine Ortix, Suwit Kiravittaya, Oliver G. Schmidt, and Jeroen van den Brink, “Curvature-induced geometric potential in strain-driven nanostructures,” *Phys. Rev. B* **84**, 045438 (2011).
- ⁷⁵ Carmine Ortix and Jeroen van den Brink, “Effect of curvature on the electronic structure and bound-state formation in rolled-up nanotubes,” *Phys. Rev. B* **81**, 165419 (2010).
- ⁷⁶ H. Aoki, M. Koshino, D. Takeda, H. Morise, and K. Kuroki, “Electronic structure of periodic curved surfaces: Topological band structure,” *Phys. Rev. B* **65**, 035102 (2001).
- ⁷⁷ Sudhakar Pandey and Carmine Ortix, “Topological end states due to inhomogeneous strains in wrinkled semiconducting ribbons,” *Phys. Rev. B* **93**, 195420 (2016).
- ⁷⁸ Fernando de Juan, Alberto Cortijo, and María A. H. Vozmediano, “Charge inhomogeneities due to smooth ripples in graphene sheets,” *Phys. Rev. B* **76**, 165409 (2007).
- ⁷⁹ Jannik C. Meyer, A. K. Geim, M. I. Katsnelson, K. S. Novoselov, T. J. Booth, and S. Roth, “The structure of suspended graphene sheets,” *Nature* **446**, 60–63 (2007).
- ⁸⁰ J. Martin, N. Akerman, G. Ulbricht, T. Lohmann, J. H. Smet, K. von Klitzing, and A. Yacoby, “Observation of electron-hole puddles in graphene using a scanning single-electron transistor,” *Nature Physics* **4**, 144–148 (2008).
- ⁸¹ Fernando de Juan, Mauricio Sturla, and María A. H. Vozmediano, “Space dependent fermi velocity in strained graphene,” *Phys. Rev. Lett.* **108**, 227205 (2012).
- ⁸² F. Guinea, M. I. Katsnelson, and A. K. Geim, “Energy gaps and a zero-field quantum hall effect in graphene by strain engineering,” *Nature Physics* **6**, 30–33 (2010).
- ⁸³ N. Levy, S. A. Burke, K. L. Meaker, M. Panlasigui, A. Zettl, F. Guinea, A. H. Castro Neto, and M. F. Crommie, “Strain-induced pseudo-magnetic fields greater than 300 tesla in graphene nanobubbles,” *Science* **329**, 544–547 (2010).
- ⁸⁴ Yuhang Jiang, Jinhai Mao, Junxi Duan, Xinyuan Lai, Kenji

- Watanabe, Takashi Taniguchi, and Eva Y. Andrei, “Visualizing strain-induced pseudomagnetic fields in graphene through an hbn magnifying glass,” *Nano Letters* **17**, 2839–2843 (2017).
- ⁸⁵ Nuno J. G. Couto, Davide Costanzo, Stephan Engels, Dong-Keun Ki, Kenji Watanabe, Takashi Taniguchi, Christoph Stampfer, Francisco Guinea, and Alberto F. Morpurgo, “Random strain fluctuations as dominant disorder source for high-quality on-substrate graphene devices,” *Phys. Rev. X* **4**, 041019 (2014).
- ⁸⁶ Daniel J. Rizzo, Sara Shabani, Bjarke S. Jessen, Jin Zhang, Alexander S. McLeod, Carmen Rubio-Verdú, Francesco L. Ruta, Matthew Cothrine, Jiaqiang Yan, David G. Mandrus, Stephen E. Nagler, Angel Rubio, James C. Hone, Cory R. Dean, Abhay N. Pasupathy, and D. N. Basov, “Nanometer-scale lateral p–n junctions in graphene/ α -rucl₃ heterostructures,” *Nano Letters*, *Nano Letters* **22**, 1946–1953 (2022).
- ⁸⁷ Yuan Cao, Valla Fatemi, Ahmet Demir, Shiang Fang, Spencer L. Tomarken, Jason Y. Luo, Javier D. Sanchez-Yamagishi, Kenji Watanabe, Takashi Taniguchi, Efthimios Kaxiras, Ray C. Ashoori, and Pablo Jarillo-Herrero, “Correlated insulator behaviour at half-filling in magic-angle graphene superlattices,” *Nature* **556**, 80–84 (2018).
- ⁸⁸ Inti Sodemann and Liang Fu, “Quantum nonlinear hall effect induced by berry curvature dipole in time-reversal invariant materials,” *Phys. Rev. Lett.* **115**, 216806 (2015).
- ⁸⁹ Su-Yang Xu, Qiong Ma, Huitao Shen, Valla Fatemi, Sanfeng Wu, Tay-Rong Chang, Guoqing Chang, Andrés M. Mier Valdivia, Ching-Kit Chan, Quinn D. Gibson, Jiadong Zhou, Zheng Liu, Kenji Watanabe, Takashi Taniguchi, Hsin Lin, Robert J. Cava, Liang Fu, Nuh Gedik, and Pablo Jarillo-Herrero, “Electrically switchable berry curvature dipole in the monolayer topological insulator wte₂,” *Nature Physics* **14**, 900–906 (2018).
- ⁹⁰ Qiong Ma, Su-Yang Xu, Huitao Shen, David MacNeill, Valla Fatemi, Tay-Rong Chang, Andrés M. Mier Valdivia, Sanfeng Wu, Zongzheng Du, Chuang-Han Hsu, Shiang Fang, Quinn D. Gibson, Kenji Watanabe, Takashi Taniguchi, Robert J. Cava, Efthimios Kaxiras, Hai-Zhou Lu, Hsin Lin, Liang Fu, Nuh Gedik, and Pablo Jarillo-Herrero, “Observation of the nonlinear hall effect under time-reversal-symmetric conditions,” *Nature* **565**, 337–342 (2019).
- ⁹¹ Yang Zhang and Liang Fu, “Terahertz detection based on nonlinear hall effect without magnetic field,” *Proceedings of the National Academy of Sciences* **118** (2021).
- ⁹² M. Kläui, C. Vaz, L. Heyderman, U. Rüdiger, and J. Bland, “Spin switching phase diagram of mesoscopic ring magnets,” *Journal of Magnetism and Magnetic Materials* **290-291**, 61–67 (2005), proceedings of the Joint European Magnetic Symposia (JEMS’ 04).
- ⁹³ O. M. Volkov, A. Kákay, F. Kronast, I. Mönch, J. Fassbender M.-A. Mawass, and D. Makarov, “Experimental observation of exchange-driven chiral effects in curvilinear magnetism,” *Phys. Rev. Lett.* **123**, 077201 (2019).
- ⁹⁴ C. Phatak, A. K. Petford-Long, and O. Heinonen, “Direct observation of unconventional topological spin structure in coupled magnetic discs,” *Physical Review Letters* **108**, 067205 (2012).
- ⁹⁵ R. Streubel, P. Fischer, F. Kronast, V. P. Kravchuk, D. D. Sheka, Y. Gaididei, O. G. Schmidt, and D. Makarov, “Magnetism in curved geometries (Topical Review),” *Journal of Physics D: Applied Physics* **49**, 363001 (2016).
- ⁹⁶ W. Jung, Y.-H. Jung, P. V. Pikhitsa, J. Feng, Y. Yang, M. Kim, H.-Y. Tsai, T. Tanaka, J. Shin, K.-Y. Kim, H. Choi, J. Rho, and M. Choi, “Three-dimensional nanoprinting via charged aerosol jets,” *Nature* **592**, 54–59 (2021).
- ⁹⁷ L. Skoric, D. Sanz-Hernández, F. Meng, C. Donnelly, S. Merino-Aceituno, and A. Fernández-Pacheco, “Layer-by-layer growth of complex-shaped three-dimensional nanostructures with focused electron beams,” *Nano Letters* **20**, 184–191 (2020).
- ⁹⁸ F. Meng, C. Donnelly, C. Abert, L. Skoric, S. Holmes, Z. Xiao, J.-W. Liao, P. J. Newton, C. H. Barnes, D. Sanz-Hernández, A. Hierro-Rodríguez, D. Suess, R. P. Cowburn, and A. Fernández-Pacheco, “Non-planar geometrical effects on the magnetoelectrical signal in a three-dimensional nanomagnetic circuit,” *ACS Nano* (2021).
- ⁹⁹ J. A. Rogers, M. G. Lagally, and R. G. Nuzzo, “Synthesis, assembly and applications of semiconductor nanomembranes,” *Nature* **477**, 45–53 (2011).
- ¹⁰⁰ O. G. Schmidt and K. Eberl, “Nanotechnology: Thin solid films roll up into nanotubes,” *Nature* **410**, 168 (2001).
- ¹⁰¹ Elliot J. Smith, Denys Makarov, Samuel Sanchez, Vladimir M. Fomin, and Oliver G. Schmidt, “Magnetic microhelix coil structures,” *Phys. Rev. Lett.* **107**, 097204 (2011).
- ¹⁰² Xueping Cui, Zhizhi Kong, Enlai Gao, Dazhen Huang, Yang Hao, Hongguang Shen, Chong-an Di, Zhiping Xu, Jian Zheng, and Daoben Zhu, “Rolling up transition metal dichalcogenide nanoscrolls via one drop of ethanol,” *Nature Communications* **9**, 1301 (2018).
- ¹⁰³ D. Grimm, C. C. B. Bufon, C. Deneke, P. Atkinson, D. J. Thurmer, F. Schäffel, S. Gorantla, A. Bachmatiuk, and O. G. Schmidt, “Rolled-up nanomembranes as compact 3d architectures for field effect transistors and fluidic sensin applications,” *Nano Letters* **13**, 213–218 (2012).
- ¹⁰⁴ C. Müller, C. C. B. Bufon, D. Makarov, L. E. Fernandez-Outon, W. A. A. Macedo, O. G. Schmidt, and D. H. Mosca, “Tuning giant magnetoresistance in rolled-up Co–Cu nanomembranes by strain engineering,” *Nanoscale* **4** (2012).
- ¹⁰⁵ D. J. Thurmer, C. C. Bof B., C. Deneke, and O. G. Schmidt, “Nanomembrane-based mesoscopic superconducting hybrid junctions,” *Nano Letters* **10**, 3704–3709 (2010).
- ¹⁰⁶ R. Streubel, D. Makarov, F. Kronast, V. Kravchuk, M. Albrecht, and O. G. Schmidt, “Magnetic vortices on closely packed spherically curved surfaces,” *Physical Review B* **85**, 174429 (2012).
- ¹⁰⁷ Sheng Xu, Zheng Yan, Kyung-In Jang, Wen Huang, Haoran Fu, Jeonghyun Kim, Zijun Wei, Matthew Flavin, Joselle McCracken, Renhan Wang, Adina Badea, Yuhao Liu, Dongqing Xiao, Guoyan Zhou, Jungwoo Lee, Ha Uk Chung, Huanyu Cheng, Wen Ren, Anthony Banks, Xiuling Li, Ungyu Paik, Ralph G. Nuzzo, Yonggang Huang, Yihui Zhang, and John A. Rogers, “Assembly of micro/nanomaterials into complex, three-dimensional architectures by compressive buckling,” *Science* **347**, 154–159 (2015).
- ¹⁰⁸ Y.-P. Zhao, D.-X. Ye, G.-C. Wang, and T.-M. Lu, “Novel nanocolumn and nano-flower arrays by glancing angle deposition,” *Nano Letters* **2**, 351–354 (2002).
- ¹⁰⁹ J. G. Gibbs, A. G. Mark, T.-C. Lee, S. Eslami, D. Schamel, and P. Fischer, “Nanohelices by shadow growth,” *Nanoscale* **6**, 9457 (2014).
- ¹¹⁰ S. Eslami, J. G. Gibbs, Y. Rechkemmer, J. van Slageren, M. Alarcón-Correa, T.-C. Lee, A. G. Mark, G. L. J. A. Rikken, and P. Fischer, “Chiral nanomagnets,” *ACS Photonics* **1**, 1231–1236 (2014).
- ¹¹¹ G. Williams, M. Hunt, B. Boehm, A. May, M. Taverne, D. Ho, S. Giblin, D. Read, J. Rarity, R. Allenspach, and S. Ladak, “Two-photon lithography for 3D magnetic nanostructure fabrication,” *Nano Research* **11**, 845–854 (2018).
- ¹¹² M. Hunt, M. Taverne, J. Askey, A. May, A. V. D. Berg, Y.-L. D. Ho, J. Rarity, and S. Ladak, “Harnessing multi-photon absorption to produce three-dimensional magnetic structures at the nanoscale,” *Materials* **13**, 761 (2020).

- ¹¹³ J. M. D. Teresa, A. Fernández-Pacheco, R. Córdoba, L. Serrano-Ramón, S. Sangiao, and M. R. Ibarra, “Review of magnetic nanostructures grown by focused electron beam induced deposition (FEBID),” *Journal of Physics D: Applied Physics* **49**, 243003 (2016).
- ¹¹⁴ M. Huth, F. Porriati, and O. Dobrovolskiy, “Focused electron beam induced deposition meets materials science,” *Microelectronic Engineering* **185-186**, 9–28 (2018).
- ¹¹⁵ R. Streubel, F. Kronast, P. Fischer, D. Parkinson, O. G. Schmidt, and D. Makarov, “Retrieving spin textures on curved magnetic thin films with full-field soft X-ray microscopies,” *Nature Communications* **6**, 7612 (2015).
- ¹¹⁶ D. Wolf, N. Biziere, S. Sturm, D. Reyes, T. Wade, T. Niermann, J. Krehl, B. Warot-Fonrose, B. Büchner, E. Snoeck, C. Gatel, and A. Lubk, “Holographic vector field electron tomography of three-dimensional nanomagnets,” *Communications Physics* **2**, 87 (2019).
- ¹¹⁷ O. M. Volkov, U. K. Rössler, J. Fassbender, and D. Makarov, “Concept of artificial magnetoelectric materials via geometrically controlling curvilinear helimagnets,” *Journal of Physics D: Applied Physics* **52**, 345001 (2019).
- ¹¹⁸ Denys Makarov, Oleksii M. Volkov, Attila Kákay, Oleksandr V. Pylypovskyi, Barbora Budinská, and Oleksandr V. Dobrovolskiy, “New dimension in magnetism and superconductivity: 3d and curvilinear nanoarchitectures,” *Advanced Materials* **34**, 2101758 (2022).
- ¹¹⁹ Claire Donnelly, Aurelio Hierro-Rodríguez, Claas Abert, Katharina Witte, Luka Skoric, Dédalo Sanz-Hernández, Simone Finizio, Fanfan Meng, Stephen McVitie, Jörg Raabe, Dieter Suess, Russell Cowburn, and Amalio Fernández-Pacheco, “Complex free-space magnetic field textures induced by three-dimensional magnetic nanostructures,” *Nature Nanotechnology* **17**, 136–142 (2022).
- ¹²⁰ J. Grollier, D. Querlioz, K. Y. Camsari, K. Everschor-Sitte, S. Fukami, and M. D. Stiles, “Neuromorphic spintronics,” *Nature Electronics* **3**, 360–370 (2020).
- ¹²¹ Oleksandr V. Pylypovskyi, Denys Y. Kononenko, Kostiantyn V. Yershov, Ulrich K. Rößler, Artem V. Tomilo, Jürgen Fassbender, Jeroen van den Brink, Denys Makarov, and Denis D. Sheka, “Curvilinear one-dimensional antiferromagnets,” *Nano Letters*, *Nano Letters* **20**, 8157–8162 (2020).
- ¹²² Dmytro Pesin and Allan H. MacDonald, “Spintronics and pseudospintronics in graphene and topological insulators,” *Nature Materials* **11**, 409–416 (2012).
- ¹²³ Andrew J. Mannix, Andrew Ye, Suk Hyun Sung, Ariana Ray, Fauzia Mujid, Chibeom Park, Myungjae Lee, Jong-Hoon Kang, Robert Shreiner, Alexander A. High, David A. Muller, Robert Hovden, and Jiwoong Park, “Robotic four-dimensional pixel assembly of van der Waals solids,” *Nature Nanotechnology* **17**, 361–366 (2022).
- ¹²⁴ Giovanni Zamborlini, Mighfar Imam, Laerte L. Patera, Tefik Onur Menteş, Nataša Stojić, Cristina Africh, Alessandro Sala, Nadia Binggeli, Giovanni Comelli, and Andrea Locatelli, “Nanobubbles at gpa pressure under graphene,” *Nano Letters*, *Nano Letters* **15**, 6162–6169 (2015).
- ¹²⁵ E. Khestanova, F. Guinea, L. Fumagalli, A. K. Geim, and I. V. Grigorieva, “Universal shape and pressure inside bubbles appearing in van der Waals heterostructures,” *Nature Communications* **7**, 12587 (2016).
- ¹²⁶ Renan Villarreal, Pin-Cheng Lin, Fahim Faraji, Nasim Hassani, Harsh Bana, Zviadi Zarkua, Maya N. Nair, Hung-Chieh Tsai, Manuel Auge, Felix Junge, Hans C. Hofsaess, Stefan De Gendt, Steven De Feyter, Steven Brems, E. Harriet Åhlgren, Erik C. Neyts, Lucian Covaci, François M. Peeters, Mehdi Neek-Amal, and Lino M. C. Pereira, “Breakdown of universal scaling for nanometer-sized bubbles in graphene,” *Nano Letters*, *Nano Letters* **21**, 8103–8110 (2021).
- ¹²⁷ Ching-Hao Chang, Jeroen van den Brink, and Carmine Ortix, “Strongly anisotropic ballistic magnetoresistance in compact three-dimensional semiconducting nanoarchitectures,” *Phys. Rev. Lett.* **113**, 227205 (2014).
- ¹²⁸ Alexander Szameit, Felix Dreisow, Matthias Heinrich, Robert Keil, Stefan Nolte, Andreas Tünnermann, and Stefano Longhi, “Geometric potential and transport in photonic topological crystals,” *Phys. Rev. Lett.* **104**, 150403 (2010).
- ¹²⁹ Michał Papaj and Liang Fu, “Magnus hall effect,” *Phys. Rev. Lett.* **123**, 216802 (2019).
- ¹³⁰ Nathan Schine, Albert Ryou, Andrey Gromov, Ariel Sommer, and Jonathan Simon, “Synthetic Landau levels for photons,” *Nature* **534**, 671–675 (2016).
- ¹³¹ T. Can, Y. H. Chiu, M. Laskin, and P. Wiegmann, “Emergent conformal symmetry and geometric transport properties of quantum hall states on singular surfaces,” *Phys. Rev. Lett.* **117**, 266803 (2016).
- ¹³² T. C. van Thiel, W. Brzezicki, C. Autieri, J. R. Hortensius, D. Afanasiev, N. Gauquelin, D. Jannis, N. Janssen, D. J. Groenendijk, J. Fatermans, S. Van Aert, J. Verbeeck, M. Cuoco, and A. D. Caviglia, “Coupling charge and topological reconstructions at polar oxide interfaces,” *Phys. Rev. Lett.* **127**, 127202 (2021).
- ¹³³ Deborah M. Paskiewicz, Rebecca Sichel-Tissot, Evguenia Karapetrova, Liliana Stan, and Dillon D. Fong, “Single-crystalline srRuO₃ nanomembranes: A platform for flexible oxide electronics,” *Nano Letters*, *Nano Letters* **16**, 534–542 (2016).
- ¹³⁴ Marios Hadjimichael, Yaqi Li, Edoardo Zatterin, Gilbert A. Chahine, Michele Conroy, Kalani Moore, Eoghan N. O’Connell, Petr Ondrejko, Pavel Marton, Jiri Hlinka, Ursel Bangert, Steven Leake, and Pavlo Zubko, “Metal-ferroelectric supercrystals with periodically curved metallic layers,” *Nature Materials* **20**, 495–502 (2021).
- ¹³⁵ Maria Teresa Mercaldo, Carmine Ortix, Francesco Giazotto, and Mario Cuoco, “Orbital vortices in *s*-wave spin-singlet superconductors in zero magnetic field,” *Phys. Rev. B* **105**, L140507 (2022).
- ¹³⁶ Tom Laeven, Bas Nijholt, Michael Wimmer, and Anton R. Akhmerov, “Enhanced proximity effect in zigzag-shaped Majorana Josephson junctions,” *Phys. Rev. Lett.* **125**, 086802 (2020).
- ¹³⁷ H. Jensen and H. Koppe, “Quantum mechanics with constraints,” *Annals of Physics* **63**, 586–591 (1971).
- ¹³⁸ R. C. T. da Costa, “Quantum mechanics of a constrained particle,” *Phys. Rev. A* **23**, 1982–1987 (1981).
- ¹³⁹ Carmine Ortix, “Quantum mechanics of a spin-orbit coupled electron constrained to a space curve,” *Phys. Rev. B* **91**, 245412 (2015).
- ¹⁴⁰ Volodymyr P. Kravchuk, Ulrich K. Rößler, Oleksii M. Volkov, Denis D. Sheka, Jeroen van den Brink, Denys Makarov, Hagen Fuchs, Hans Fangohr, and Yuri Gaididei, “Topologically stable magnetization states on a spherical shell: Curvature-stabilized skyrmions,” *Phys. Rev. B* **94**, 144402 (2016).
- ¹⁴¹ Yasuhiro Asano, “Josephson spin current in triplet superconductor junctions,” *Phys. Rev. B* **74**, 220501 (2006).